DISSERTAÇÃO DE MESTRADO IFT–D.004/2026

AdS/CMT Thermal and Quantum Phase Transitions and self-duality

Diego Matias Cazón Tejerina

Orientador

Horatiu Nastase

Maio de 2026

Cazón Tejerina, Diego Matias
C386a AdS/CMT thermal and quantum phase transitions and self-duality / Diego Matias Cazón Tejerina. – São Paulo, 2026
68 f: il. color.

Dissertação (mestrado) – Universidade Estadual Paulista (Unesp), Instituto de Física Teórica (IFT), São Paulo
Orientador: Horatiu Nastase

1. Teoria de campos (Física). 2. Matéria condensada. 3.Supercondutividade. I. Título

Sistema de geração automática de fichas catalográficas da Unesp. Biblioteca do Instituto de Física Teórica (IFT), São Paulo. Dados fornecidos pelo autor(a).

ADS/CMT THERMAL AND QUANTUM PHASE TRANSITIONS AND SELF-DUALITY

Dissertação de Mestrado apresentada ao Instituto de Física Teórica do Câmpus de São Paulo, da Universidade Estadual Paulista “Júlio de Mesquita Filho”, como parte dos requisitos para obtenção do título Mestre em Ciências, área: Física.

Comissão Examinadora:

Profa. Dra. HORATIU NASTASE (Orientador)
Instituto de Física Teórica/UNESP

Prof. Dr. DARIO ROSA
Instituto de Física Teórica/UNESP

Prof. Dr. DMITRY MELNIKOV
Instituto Internacional de Física, Universidade Federal do Rio Grande do Norte (IIP/UFRN)

Conceito: Aprovado

São Paulo, 07 de maio de 2026.

Dedico esta tese
aos meus pais, Carlos e Rosa,
e à minha esposa, Sami,
pelo amor e apoio incondicional.

Acknowledgments

I begin by thanking the Lord. My gratitude is immense and goes beyond what words can express; He has been my source of strength and wisdom throughout this entire journey.

I would like to express my deepest gratitude to my advisor, Professor Horatiu Nastase. He is one of the sharpest minds I have had the privilege to know, and his vast knowledge has been truly inspiring. I have learned an immense amount from him, not only through his mentorship but also through his wonderful textbooks and unique teaching methods. I am particularly grateful for his crucial support in securing the FAPESP scholarship and for his invaluable guidance and recommendation regarding the next steps of my career.

I thank the Instituto de Física Teórica (IFT-UNESP) for providing a stimulating environment for research. I acknowledge the essential financial support provided by CAPES (Process 88887.947464/2024-00) throughout this process, as well as the support from FAPESP (Process 2024/13212-0), which was vital for my research.

To my family, thank you for your unwavering support from the very beginning. I am forever grateful for the sacrifices you made to send me from Sucre to La Paz to begin my journey in physics. Your belief in me has made all of this possible.

I would also like to thank my friends at IFT for their camaraderie. Special thanks to Yhoni, Dennis, Milton, Gabriel, Fernando, Joel, among many others, for the excellent company during lunch breaks, where our discussions about physics—and everything else—provided a much-needed respite and fresh perspective.

Finally, to my wife: thank you for being the best company I could ever ask for. You made every moment of our life in São Paulo wonderful, and this achievement is as much yours as it is mine.

Agradecimientos

Comienzo agradeciendo al Señor. Mi gratitud es inmensa y va más allá de lo que las palabras pueden expresar; Él ha sido mi fuente de fortaleza y sabiduría a lo largo de todo este camino.

Quisiera expresar mi más profundo agradecimiento a mi director, el Profesor Horatiu Nastase. Es una de las mentes más brillantes que he tenido el privilegio de conocer, y su vasto conocimiento ha sido verdaderamente inspirador. He aprendido enormemente de él, no solo a través de su mentoría, sino también mediante sus excelentes libros y sus métodos de enseñanza únicos. Estoy especialmente agradecido por su apoyo crucial para obtener la beca de FAPESP y por su valiosa orientación y recomendación respecto a los siguientes pasos de mi carrera.

Agradezco al Instituto de Física Teórica (IFT-UNESP) por proporcionar un ambiente estimulante para la investigación. Reconozco el apoyo financiero esencial brindado por CAPES (Proceso 88887.947464/2024-00) durante este período, así como el apoyo de FAPESP (Proceso 2024/13212-0), que fue vital para mi investigación.

A mi familia, gracias por su apoyo incondicional desde el principio. Les estaré siempre agradecido por los sacrificios que hicieron para enviarme de Sucre a La Paz e iniciar mi camino en la física. Su confianza en mí hizo posible todo esto.

También quisiera agradecer a mis amigos del IFT por su compañerismo. Un agradecimiento especial a Yhoni, Dennis, Milton, Gabriel, Fernando, Joel, entre muchos otros, por la excelente compañía durante los almuerzos, en los que nuestras conversaciones sobre física —y sobre todo lo demás— me brindaron un respiro necesario y una perspectiva renovada.

Por último, a mi esposa: gracias por ser la mejor compañía que podría haber soñado. Hiciste que cada momento de nuestra vida en São Paulo fuera maravilloso, y este logro es tan tuyo como mío.

"Caeli enarrant gloriam Dei,
et opera manuum eius annuntiat firmamentum."

Psalmi 18:2 (Vulgata)

Resumo

Esta tese investiga as propriedades termodinâmicas e de transporte de supercondutores holográficos para além das restrições impostas pela auto-dualidade eletromagnética padrão. Consideramos um modelo de Einstein–Maxwell–escalar em AdS_4 deformado por um acoplamento de Weyl com derivadas mais altas. O coeficiente de Weyl γ atua como um parâmetro de controle físico que ajusta o comportamento crítico no infravermelho da teoria de campo dual, de forma qualitativamente análoga a como densidade de portadores, desordem ou pressão ajustam fases em sistemas de matéria condensada. Ao renormalizar interações efetivas na geometria de horizonte próximo AdS_2, o termo de Weyl desloca o limite de estabilidade de Breitenlohner–Freedman e conduz o sistema através de uma superfície quântica crítica. Esse mecanismo gera naturalmente uma transição do tipo Berezinskii–Kosterlitz–Thouless (BKT) de ordem infinita para o parâmetro de ordem supercondutor, oferecendo uma alternativa geometricamente consistente a deformações ad hoc de massa para modelar criticidade não–média–de–campo.

Além disso, a interação de Weyl quebra a auto-dualidade eletromagnética inerente às teorias de Maxwell no bulk. Mostramos que essa quebra induz uma assimetria partícula–vórtice ajustável na condutividade óptica, conectando o mesmo acoplamento γ que controla a instabilidade no IR a um viés controlado no transporte quântico crítico—características relevantes para a fenomenologia de metais estranhos. Em conjunto, esses resultados ilustram uma lição mais ampla para a holografia: termos com derivadas mais altas que aparecem como pequenas correções no ultravioleta podem reorganizar qualitativamente a física no infravermelho, tornando-se ferramentas poderosas para capturar a dinâmica universal de matéria quântica fortemente acoplada.

Palavras Chaves: Dualidade calibre/gravidade; Supercondutores holográficos; Correção de Weyl; AdS/CMT; Criticalidade quântica.

Áreas do conhecimento: Física de Partículas e Campos; Matéria Condensada.

Abstract

This thesis investigates the thermodynamic and transport properties of holographic superconductors beyond the constraints imposed by standard electromagnetic self-duality. We focus on an Einstein–Maxwell–scalar model in AdS_4 deformed by a higher-derivative Weyl coupling. The Weyl coefficient γ acts as a physical control parameter that tunes the infrared critical behavior of the dual field theory, in a way qualitatively analogous to how carrier density, disorder, or pressure tune phases in condensed matter systems. By renormalizing effective interactions in the near-horizon AdS_2 geometry, the Weyl term shifts the Breitenlohner–Freedman stability bound and drives the system across a quantum critical surface. This mechanism naturally generates an infinite-order Berezinskii–Kosterlitz–Thouless (BKT)–type transition for the superconducting order parameter, providing a geometrically consistent alternative to ad hoc mass deformations for modeling non–mean–field criticality.

Furthermore, the Weyl interaction breaks the electromagnetic self-duality inherent in standard bulk Maxwell theories. We show that this breaking induces a tunable particle–vortex asymmetry in the optical conductivity, linking the same coupling γ that controls the IR instability to a controlled bias in quantum critical transport—features relevant to the phenomenology of strange metals. Taken together, these results illustrate a broader lesson for holography: higher-derivative terms that appear as small ultraviolet corrections can qualitatively reorganize the infrared physics, making them powerful tools for capturing universal dynamics in strongly coupled quantum matter.

Keywords: Gauge/gravity duality. Holographic superconductors. Weyl correction. AdS/CMT. Quantum criticality.

Knowledge Areas: Physics of Particles and Fields; Condensed Matter.

Contents

Chapter 1

Introduction

1.1 Gauge/Gravity Duality and Strong Coupling

String theory was originally formulated as a theory of the oscillation modes of a fundamental string, whose excitations represent all particles in nature (the known ones and many others). Because it contains a massless spin–2 excitation identified with the graviton, it also provides a perturbatively consistent quantum theory of gravity. One of its most remarkable outcomes is the AdS/CFT correspondence, first proposed by Maldacena [1] (see [2] for a review), which relates string or gravitational theories on asymptotically anti–de Sitter (AdS) backgrounds to non–gravitational quantum field theories (QFTs) living on their boundary. In this gauge/gravity duality, a strongly coupled QFT in d dimensions is mapped to a weakly coupled gravitational theory in $d+1$ dimensions, providing a nonperturbative tool to study regimes where standard field–theory methods fail.

1.2 AdS/CMT and Strongly Coupled Matter

Over the last two decades this idea has been applied to condensed–matter physics under the name AdS/CMT (AdS/condensed–matter) correspondence. The basic philosophy is bottom–up: one writes down an effective gravitational theory in AdS such that, via the holographic dictionary, it reproduces key qualitative features of a strongly coupled quantum many–body system [3]. Once the bulk action and boundary conditions are specified, correlation functions, transport coefficients and phase structures on the QFT side are obtained by solving classical equations of motion in the bulk. This makes holography a natural framework to model systems without long–lived quasiparticles, where perturbative approaches around a Fermi liquid break down.

1.3 Holographic Superconductors

Superconductivity provides a useful testing ground for this program. On the field-theory side, conventional superconductors can be described by Landau–Ginzburg and BCS theory, but many materials of interest, such as high-T_c cuprates, lie in regimes where fluctuations and strong coupling are essential and a simple quasiparticle picture is inadequate.

On the holographic side, a minimal model for a strongly coupled superconductor is the Einstein–Maxwell theory in AdS coupled to a charged scalar [4, 5, 6]. Above a critical temperature T_c, the scalar vanishes and the system is in the normal phase. Below T_c, the scalar becomes unstable and develops a nontrivial radial profile. In the boundary theory, this is interpreted as the spontaneous condensation of a charged operator.

This instability also has a useful infrared interpretation. In the extremal Reissner–Nordström AdS_4 solution, the near-horizon region has the form $AdS_2 \times \mathbb{R}^2$. The charged scalar becomes unstable when its effective mass violates the Breitenlohner–Freedman bound in this AdS_2 region. This infrared viewpoint will be important later when we study how the Weyl correction modifies the superconducting instability.

1.4 Weyl Corrections and Thesis Question

In the minimal Einstein–Maxwell theory in AdS_4, the Maxwell sector has a special property: its equations are invariant under an exchange of electric and magnetic fields. This is the electromagnetic self-duality of the bulk theory. In the dual (2+1)-dimensional boundary theory, this symmetry is related to particle–vortex duality.

For the optical conductivity, this self-duality is quite restrictive. Roughly speaking, the particle-like and vortex-like contributions to the response are not independent; they are tied together by the duality. As a result, the simplest Maxwell theory does not describe the most general possible frequency dependence of $\sigma(\omega)$. It gives a very useful starting point, but it is too special if one wants to model more general quantum critical transport.

A controlled way to go beyond this self-dual limit is to add a higher-derivative correction to the gauge sector. In this thesis we consider a coupling between the

Maxwell field strength and the Weyl tensor,

$$S_{\mathrm{Weyl}} \;=\; \gamma \frac{L^2}{g_4^2} \int d^4x \,\sqrt{-g}\, C_{\mu\nu\rho\sigma} F^{\mu\nu} F^{\rho\sigma}. \tag{1.1}$$

This term vanishes in pure AdS, but it becomes important in curved regions of the bulk, such as the near-horizon throat of a black brane [7, 8]. The parameter γ is dimensionless and controls the size of the correction. We restrict ourselves to the standard range of γ allowed by causality constraints in the bulk.

Turning on γ breaks the electromagnetic self-duality of the Maxwell theory. On the boundary side, this means that the particle-like and vortex-like responses are no longer forced to be symmetric. The Weyl coupling therefore gives a simple way to introduce a tunable particle–vortex asymmetry in the optical conductivity.

The aim of this thesis is to study how this Weyl correction affects two aspects of holographic superconductors.

First, we study its effect on the superconducting instability. We consider a planar Reissner–Nordström AdS_4 black brane coupled to a charged scalar, as in the minimal holographic superconductor, and add the CFF term with a small coupling γ. In the extremal limit, the near-horizon region of the charged black brane is $AdS_2 \times \mathbb{R}^2$. At low but nonzero temperature, the corresponding near-extremal region still controls the low-energy instability. The scalar becomes unstable when its effective mass violates the AdS_2 Breitenlohner–Freedman bound. We ask how the Weyl coupling changes this instability condition and the associated IR scaling exponent. Close to this threshold, the critical scale can be generated exponentially rather than by an ordinary power law. In this thesis we will refer to this behavior as Berezinskii–Kosterlitz–Thouless (BKT)-type scaling; the terminology refers mainly to the exponential scaling form, while the precise microscopic mechanism is different from the standard condensed-matter BKT transition.

Second, we study its effect on transport. For this purpose we consider Weyl-corrected Maxwell dynamics on a neutral AdS–Schwarzschild background, which provides a simple setting for computing finite-temperature optical conductivity. In this case we ask how γ deforms $\sigma(\omega)$ away from the self-dual result and how this deformation can be interpreted as particle–vortex asymmetry in the boundary theory.

Thus, the Weyl coupling is used in two related ways: it modifies the infrared instability that leads to superconductivity, and it modifies the optical response of the strongly coupled system.

1.5 Organization of the Thesis

The rest of this thesis is organized as follows. Chapter 2 reviews the AdS/CFT correspondence, first at a general level and then in its phenomenological AdS/CMT extension. Chapter 3 moves to condensed–matter physics, summarizing the Landau Fermi–liquid paradigm, its breakdown in strange metals, the role of quantum criticality and non–quasiparticle transport, and the resulting motivation for holographic models. Chapter 4 introduces the minimal holographic superconductor, including the Einstein–Maxwell–scalar setup, the condensation mechanism, and basic transport properties such as the optical conductivity and mass gap. Chapter 5 turns to Weyl corrections and quantum critical transport: we discuss higher–derivative corrections and the distinguished role of the Weyl tensor, electromagnetic self–duality and its breaking, causality bounds on the Weyl coupling γ, and top–down motivation from ABJM–inspired Landau–Ginzburg physics. Chapter 6 presents the specific bulk model used in this work, fixing the action, ansatz, equations of motion and conventions. Chapter 7 contains the IR analysis in the AdS_2 region, the computation of the IR scaling exponent, and the derivation of BKT–type scaling for the critical temperature and condensate. Chapter 8 is devoted to conductivity and transport in the presence of the Weyl coupling, from the fluctuation problem and Kubo formula to the optical conductivity and its particle–vortex interpretation. Finally, Chapter 9 summarizes our main results, discusses their condensed–matter interpretation and implications for holography, and outlines possible directions for future work.

Chapter 2

The AdS/CFT Correspondence

In this chapter we introduce only the parts of the AdS/CFT correspondence that will be used in the rest of the thesis. The goal is not to give a complete review of holography, but to fix the basic dictionary needed for the holographic superconductor model.

The main ideas are the following. Bulk fields are interpreted as sources and responses for operators in the boundary theory. The radial direction of AdS is related to the energy scale of the boundary field theory. Finally, black branes describe finite-temperature states, while bulk gauge fields and charged scalars allow us to model charge transport and condensation.

We will use these ideas in an AdS_4/CFT_3 setting, appropriate for effective 2+1-dimensional quantum systems. The material follows standard AdS/CFT reviews, in particular [2, 3].

2.1 The Holographic Dictionary

From D-branes to field theories

The AdS/CFT correspondence states, in its simplest form, that certain strongly coupled quantum field theories can be described in terms of gravitational theories in higher-dimensional anti–de Sitter (AdS) spacetimes. The original example relates type IIB string theory on $AdS_5 \times S^5$ to $\mathcal{N} = 4$ super Yang–Mills theory in 3+1 dimensions at large N and large 't Hooft coupling.

For applications to (2+1)-dimensional quantum critical systems, an important case is the ABJM theory, a 2+1-dimensional $\mathcal{N} = 6$ superconformal Chern–Simons–matter theory, which is related, in an appropriate large-N limit, to type IIA string theory on $AdS_4 \times \mathbb{C}P^3$.

These top–down constructions provide canonical *anchors*: they are the settings where the AdS/CFT correspondence is formulated most sharply and is supported by a large amount of evidence. In this thesis, however, we will mostly work with a bottom–up effective model, namely an Einstein–Maxwell–scalar theory with a Weyl correction. This model is designed to capture universal features of strongly coupled charged matter rather than to describe a particular UV-complete theory.

Sources, responses, and the bulk/boundary dictionary

The practical use of holography comes from the relation between bulk fields and boundary operators. The value of a bulk field near the AdS boundary acts as a source for an operator in the boundary theory, while the subleading behavior of the same bulk field determines the response of that operator. This is the basic reason why solving a classical equation in the bulk can give correlation functions in the boundary theory.

More precisely, the AdS/CFT dictionary relates two ways of computing the same generating functional. On the field-theory side, one studies the boundary theory in the presence of external sources. If $\mathcal{O}_i$ is an operator in the boundary theory, we can couple it to a source $\phi_i^{(0)}$. Schematically, this corresponds to deforming the field-theory action as

$$S_{\mathrm{CFT}} \;\longrightarrow\; S_{\mathrm{CFT}} + \int d^d x\, \phi_i^{(0)}(x)\, \mathcal{O}_i(x). \tag{2.1}$$

The generating functional $Z_{\mathrm{CFT}}[\{\phi_i^{(0)}\}]$ then contains the response of the theory to these sources.

On the gravity side, the same source $\phi_i^{(0)}$ is interpreted as the boundary value of a bulk field Φ_i. Thus, instead of computing the strongly coupled field theory directly, one solves the classical bulk equations with boundary condition

$$\Phi_i \to \phi_i^{(0)} \qquad \text{near the AdS boundary.} \tag{2.2}$$

The AdS/CFT prescription then states, schematically, that

$$Z_{\mathrm{CFT}}[\{\phi_i^{(0)}\}] = Z_{\mathrm{string}}[\{\Phi_i \!\to\! \phi_i^{(0)}\}] \simeq \exp\!\big(-S_{\mathrm{bulk}}^{\text{on-shell}}[\{\Phi_i \!\to\! \phi_i^{(0)}\}]\big), \tag{2.3}$$

where the last expression holds in the classical gravity limit.

The practical meaning of this formula is simple. The boundary value of a bulk field tells us which source is applied in the field theory. After solving the bulk equations with that boundary condition, the on-shell action becomes a functional of the source. Differentiating this functional with respect to the source gives the corresponding boundary correlation functions:

$$\langle \mathcal{O}_1 \cdots \mathcal{O}_n \rangle_{\text{conn}} \sim \frac{\delta^n W[\{\phi_i^{(0)}\}]}{\delta\phi_1^{(0)} \cdots \delta\phi_n^{(0)}}, \qquad W = -\log Z_{\text{CFT}} \simeq S_{\text{bulk}}^{\text{on-shell}}. \tag{2.4}$$

Here the symbol $\sim$ allows for conventional normalization factors. This is the reason why, in holography, solving a classical differential equation in the bulk can determine response functions of a strongly coupled boundary theory.

Concretely, consider a scalar field Φ of mass m in AdS$_{d+1}$. Near the boundary (radial coordinate $r \to \infty$ in Poincaré coordinates), the solution behaves as

$$\Phi(r,x) \simeq r^{-\Delta_-}\phi^{(0)}(x) + r^{-\Delta_+}\phi^{(1)}(x) + \cdots, \tag{2.5}$$

where the scaling dimensions $\Delta_\pm$ are related to the mass by

$$\Delta_\pm = \frac{d}{2} \pm \sqrt{\frac{d^2}{4} + m^2L^2}. \tag{2.6}$$

In standard quantization, the leading coefficient $\phi^{(0)}(x)$ is interpreted as the source for the dual operator $\mathcal{O}(x)$, while the subleading coefficient $\phi^{(1)}(x)$ is proportional to its expectation value.

Schematically,

$$\phi^{(0)} \leftrightarrow \text{source}, \qquad \phi^{(1)} \leftrightarrow \langle \mathcal{O} \rangle. \tag{2.7}$$

For masses above the Breitenlohner–Freedman bound, $m^2L^2 \geq -\frac{d^2}{4}$, the dimension Δ_+ defines the standard quantization. In the narrower window $-\frac{d^2}{4} \leq m^2L^2 < -\frac{d^2}{4} + 1$, both falloffs are normalizable, and one can alternatively interpret the Δ_- mode as the expectation value and Δ_+ as the source, Thus, the same bulk scalar can correspond to two different boundary theories, depending on which falloff is held fixed as the source.

Analogous statements hold for other bulk fields:

- the metric $g_{\mu\nu}$ is dual to the boundary stress tensor T_{ij};
- a bulk U(1) gauge field A_μ is dual to a conserved U(1) current J_i;
- bulk fermions are dual to fermionic operators.

The radial direction as an energy scale

A useful feature of AdS/CFT is that the radial direction in the bulk has an energy-scale interpretation in the boundary theory. In the coordinates used in this thesis, this means:

- the AdS boundary $r \to \infty$ corresponds to the UV of the CFT;
- moving inward (towards smaller r) corresponds to flowing to the IR.

Bulk fields evaluated at a finite radial cutoff encode a cutoff (Wilsonian) effective description of the CFT, i.e. the theory deformed and coarse–grained down to a corresponding energy scale. More generally, changes in the bulk geometry can encode RG flow in the boundary theory.

In the finite-temperature and finite-density setups relevant to this thesis, the IR physics is often controlled by the near-horizon region of a charged black brane. For the extremal Reissner–Nordström–AdS_4 black brane, this near-horizon geometry is $AdS_2 \times \mathbb{R}^2$. At low but nonzero temperature, the corresponding near-extremal region still gives the relevant low-energy description.

This near-horizon AdS_2 region will be important in Chapter 7, where we analyze the low-energy scalar instability.

Why AdS_4/CFT_3 is the relevant setting

Many experimentally relevant systems, such as thin films, layered materials, and surface states, are effectively 2+1–dimensional at low energies. AdS_4/CFT_3 is therefore a natural holographic setting for modeling such systems.

In this thesis, we use this setting in a bottom–up way. The basic ingredients are:

- The bulk is a four-dimensional asymptotically AdS spacetime with a planar black brane. We first review the Einstein–Maxwell–scalar model and then deform it by adding a Weyl correction. (Chapters 4 and 6).
- The boundary theory is an effective 2+1-dimensional quantum field theory at finite temperature T and finite chemical potential μ for a global U(1) charge.
- The bulk scalar ψ is dual to a charged operator $\mathcal{O}$. When this operator develops an expectation value, it plays the role of a superconducting order parameter. The bulk gauge field A_μ is dual to the conserved current J^μ.

This setup is inspired by top–down examples such as ABJM theory at finite density, whose dual includes AdS_4 geometries, but we will not rely on a specific UV completion. Instead, we view our model as a controlled effective description of a generic strongly coupled CFT_3 with a U(1) symmetry, focusing on universal IR and transport properties.

2.2 Holography as a Tool for Condensed Matter

With this dictionary in mind, holography can be used as an effective tool for strongly coupled condensed-matter systems, especially when weak-coupling or quasiparticle-based approaches are unreliable. Typical examples include:

- non–Fermi liquids and strange metals;
- quantum critical points at finite density;
- unconventional and high–T_c superconductors;
- transport in strongly correlated systems without well–defined quasiparticles.

The basic idea is to model the strongly coupled system by a dual gravitational background (often involving charged black branes, scalars, and gauge fields), using the AdS/CFT dictionary to compute observables such as:

- thermodynamic quantities from black–brane thermodynamics;
- retarded Green's functions from linearized bulk fluctuations;
- conductivities and diffusion constants from Kubo formulas;
- phase diagrams from bulk instabilities (e.g. scalar condensation).

Even though such models are highly idealized, they can capture robust features of strongly coupled dynamics, especially scaling behavior and transport without well-defined quasiparticles.

What the model captures and what it does not

It is important to stress what holography is *not* doing in this context. The bulk fields do not literally represent electrons in a specific material, and the extra AdS dimension is not a physical spatial dimension. Instead:

- The bulk geometry encodes the RG structure and the thermodynamics of the dual QFT.
- The bulk gauge field represents a global U(1) current, not an emergent dynamical photon in the condensed matter sense.
- The scalar field ψ models a charged operator that can condense. It should not be interpreted as a microscopic Cooper-pair wavefunction tied to a specific band structure or pairing mechanism.

Because of this, holographic models should be interpreted as *toy models*: simplified, strongly coupled laboratories designed to isolate and study robust features such as scaling, universality, and non–quasiparticle transport, rather than faithful microscopic models of any given compound.

Chapter 3

Condensed-Matter Motivation

In this chapter we review why the Landau–Fermi liquid (FL) paradigm fails in many strongly correlated metals, and summarize a compact set of organizing principles for *strange metals*. The emphasis is on a "quantum matter without quasiparticles" viewpoint, following the perspective of Hartnoll, Lucas and Sachdev's review of holographic quantum matter [9] together with the discussion of Fermi liquids and high-T_c superconductors in Nastase's textbook on AdS/CMT [3]. This will motivate the use of holographic models as toy descriptions of strongly coupled, non–quasiparticle transport.

The structure of the chapter is as follows. We first recall the Fermi-liquid picture, where transport is controlled by long-lived quasiparticles. We then explain why strange metals are different, and finally why holography is useful for describing transport without assuming quasiparticles.

3.1 The Reference Point: Fermi Liquids

Landau–Fermi liquid (FL) theory is the standard effective description of most conventional metals with interacting electrons. Rather than treating interactions as a small perturbation of a free Fermi gas, Landau's idea is that the interacting system can still be described in terms of long–lived low–energy *quasiparticles*: excitations that behave like weakly interacting fermions with renormalized parameters (effective mass, Fermi velocity, etc.).

In this sense, Fermi-liquid theory is powerful because it says that interactions do not completely destroy the particle-like description; they mainly change the parameters of the effective particles.

Two central assumptions can be phrased as follows [3]:

1. The dominant effect of interactions is to renormalize quantities such as the effective mass, $m \to m^*$, typically by a factor of order $10\% - 50\%$.

2. There is a one–to–one correspondence between the low–energy excited states of the interacting metal and those of a noninteracting Fermi gas. The excitations are quasiparticles which can, in principle, be complicated composites of the underlying electrons but are long–lived within the metal.

A key dynamical consequence is that the quasiparticle decay rate vanishes as energy and temperature decrease: excitations sufficiently close to the Fermi surface become increasingly long–lived, with an ever–narrower spectral peak as $\varepsilon \to \varepsilon_F$.

The physical reason is simple. Fermions obey the Pauli exclusion principle, so a quasiparticle can scatter only into final states that are not already occupied. At low temperature, the states below the Fermi surface are almost all filled, while states far above the Fermi surface require too much energy to reach. Therefore, only a thin shell of final states near the Fermi surface is available for scattering.

A simple phase–space argument makes this precise [3]. Consider the scattering of an excited quasiparticle with energy $\varepsilon_1 > \varepsilon_F$ off a quasiparticle inside the Fermi sea, $\varepsilon_2 < \varepsilon_F$, into final states with $\varepsilon_3, \varepsilon_4 > \varepsilon_F$. Energy conservation imposes

$$\varepsilon_1 + \varepsilon_2 = \varepsilon_3 + \varepsilon_4. \tag{3.1}$$

If we set $\varepsilon_1 = \varepsilon_F$, this condition forces $\varepsilon_2 = \varepsilon_3 = \varepsilon_4 = \varepsilon_F$, so the available phase space for scattering collapses. Thus, exactly at the Fermi surface, there is essentially no room for a quasiparticle to scatter while respecting both energy conservation and the Pauli principle. More generally, for $\delta\varepsilon \equiv \varepsilon_1 - \varepsilon_F > 0$, the phase space for ε_2 and ε_3 scales as $(\delta\varepsilon)^2$. The scattering rate, proportional to the density of final states, behaves as

$$\tau^{-1} \propto (\varepsilon_1 - \varepsilon_F)^2. \tag{3.2}$$

If the excitation is thermal, $\varepsilon_1 - \varepsilon_F \sim k_B T$, then

$$\tau^{-1} \propto T^2, \tag{3.3}$$

so quasiparticles become increasingly long–lived as $T \to 0$.

This is the key point: in a Fermi liquid, the low-temperature limit is a regime of increasingly sharp and well-defined excitations.

When momentum relaxation is present (e.g. from impurities), the same phase–space structure implies a characteristic Fermi–liquid resistivity

$$\rho(T) \propto T^2, \tag{3.4}$$

over an appropriate low–temperature window. This T^2 law is one of the most robust experimental fingerprints of Fermi–liquid behavior: it expresses the fact that low–energy quasiparticles are long–lived and that scattering is strongly phase–space suppressed near the Fermi surface.

The T^2 resistivity is therefore the standard behavior expected when long-lived quasiparticles control transport.

However, many strongly correlated materials do not follow this pattern. Most famously, the normal state of high–T_c cuprate superconductors shows a resistivity that is approximately linear in T, $\rho(T) \propto T$, over wide temperature ranges above T_c, with no clear crossover to the Fermi–liquid law (3.4) as $T \to T_c$. Spectral probes also display broad, incoherent excitations rather than sharp, long–lived quasiparticle peaks. These regimes are commonly referred to as *strange metals*. They suggest that the quasiparticle picture, which works so well for Fermi liquids, is no longer the right starting point.

3.2 When Quasiparticles Are Not Enough

A more precise way to characterize "no quasiparticles" is to focus on dynamical timescales, following the discussion in [9].

The basic idea is that a quasiparticle description is useful only when the excitations live long enough to behave as identifiable objects. If the system relaxes too quickly, the notion of a long-lived quasiparticle loses its meaning.

Consider a system slightly perturbed away from thermal equilibrium at temperature T. If quasiparticles exist, the perturbation creates a dilute gas of long–lived excitations that collide and slowly establish *local* equilibrium. Let τ_φ denote the local equilibration, or dephasing, time: the time scale over which a small perturbation relaxes and can no longer be described as a coherent long-lived excitation.

In familiar settings with quasiparticles, τ_φ becomes parametrically long at low T. For instance, in a Fermi liquid a standard Fermi–golden–rule computation yields $\tau_\varphi \sim 1/T^2$, while in a gapped system one finds $\tau_\varphi \sim e^{\Delta/T}$ due to the exponential suppression of thermal excitations. By contrast, in quantum matter without quasiparticles one expects τ_φ to be as short as it can consistently be. A broad set of arguments and model examples suggest a lower bound of the form

$$\tau_\varphi \;\geq\; C\,\frac{\hbar}{k_B T}, \qquad C = \mathcal{O}(1),. \tag{3.5}$$

A useful diagnostic of quantum matter without long-lived quasiparticles is then that the relaxation time is of this order, $\tau_\varphi \sim \hbar/(k_B T)$, rather than being parametrically longer. This time scale is often called the Planckian time. It is not a microscopic constant; rather, it is the natural quantum time scale set by the temperature T. Thus, when the relaxation time is of this order, the system relaxes on the fast thermal time scale expected for a strongly coupled system.

A closely related dynamical concept comes from quantum chaos. One can define a Lyapunov time τ_L from the exponential growth regime of suitably chosen out–of–time–order correlators; under mild assumptions, Maldacena, Shenker, and Stanford showed that [10]

$$\tau_L \;\geq\; \frac{1}{2\pi}\,\frac{\hbar}{k_B T}, \tag{3.6}$$

and holographic black holes and SYK–like models saturate this bound. From this viewpoint, strange metals should not be thought of simply as ordinary Fermi liquids with stronger scattering. Rather, they are examples of strongly coupled systems in which local equilibration and chaotic dynamics occur on thermal time scales of order $\hbar/(k_B T)$.

3.3 Strange metals and high-T_c superconductors

One of the main physical motivations for quantum matter without quasiparticles comes from high-T_c superconducting materials. These materials typically (i) have critical temperatures above that of liquid nitrogen, (ii) are mostly cuprates (copper oxides), and (iii) are layered, so that the electronic dynamics is effectively $2+1$-dimensional. There are also organic compounds with similar phenomenology [3].

The reason these systems are relevant here is that their normal state, above the superconducting transition, often displays strange-metal behavior rather than ordinary Fermi-liquid behavior.

An important indication of strong coupling in these systems is the ratio $2\Delta/(k_B T_c)$: instead of the BCS value $\simeq 3.52$ appropriate for weak–coupling, conventional superconductors, in cuprates this ratio is larger by a factor of order two, signalling that ordinary weak–coupling theory is insufficient and that a new, intrinsically strongly coupled description is needed.

Figure 3.1 shows the standard schematic (T, x) phase diagram of the cuprates, where x denotes the doping (viewed as a tuning parameter). Here x measures

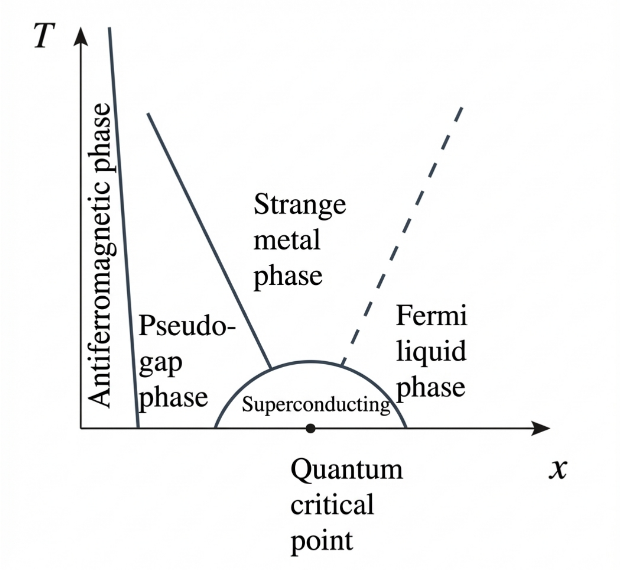

Figura 3.1: Schematic (T, x) phase diagram of a high-T_c cuprate, illustrating the antiferromagnetic, pseudogap, superconducting, strange–metal, and overdoped Fermi–liquid–like regimes.

how many charge carriers are added to the parent insulating compound. Changing x changes the ground state of the material, so it plays the role of a control parameter. For our purposes, the key feature is the extended "strange–metal" regime above the superconducting dome, often drawn as a V–shaped quantum–critical fan. This regime is termed "strange" because it does *not* obey conventional Fermi–liquid theory and is therefore frequently described as a non–Fermi liquid. Heavy–fermion compounds exhibit closely related strange–metal phenomenology (typically without a pseudogap), with an effective mass that can be enhanced by orders of magnitude.

From the transport point of view, the key contrast between Fermi liquids and strange metals is particularly sharp. For a Fermi liquid, the low–temperature thermodynamics and resistivity behave as

$$C_e \simeq \gamma T + \dots, \qquad \gamma \propto m^*, \tag{3.7}$$

$$\rho_e(T) = \rho_0 + AT^2 + \dots, \tag{3.8}$$

almost independently of microscopic details: the specific heat is linear in T, and the resistivity is quadratic, reflecting long–lived quasiparticles and the phase–space suppression of scattering near the Fermi surface (cf. (3.4)). By contrast, in the strange–metal phase of high-T_c superconductors one finds

$$\rho_e(T) = B\,T + \ldots, \qquad T > T_c, \tag{3.9}$$

over a wide temperature range above the superconducting transition, with no clear crossover to a T^2 law. This robust, nearly linear resistivity is one of the central experimental signatures of strange–metal behavior.

This behavior is surprising because it does not follow the Fermi-liquid pattern. In a Fermi liquid, scattering becomes strongly suppressed at low temperature, leading to $\rho(T) \propto T^2$. In a strange metal, the approximately linear law $\rho(T) \propto T$ indicates a much faster relaxation of charge transport.

The single-particle viewpoint makes the breakdown of quasiparticles more explicit. A useful way to describe this is through the retarded Green's function. Physically, this Green's function tells us whether adding an electron creates a sharp, long-lived excitation or a broad, rapidly decaying one:

$$G^R(\omega,k) \;\sim\; \frac{1}{\omega - v_F(k-k_F) + \Sigma(\omega,k)}, \tag{3.10}$$

where $\Sigma(\omega,k)$ is the self-energy. For a Fermi liquid one finds

$$\Sigma_{\mathrm{FL}}(\omega) \;\sim\; i\,\omega^2, \tag{3.11}$$

so that the decay rate $\Gamma \sim -2\,\Im\Sigma$ is quadratic in frequency (and in temperature for thermal excitations). Since the imaginary part of the self-energy measures the decay rate, this means that the decay rate becomes very small at low frequency. This leads to a narrow quasiparticle peak: excitations are long-lived and propagate coherently.

In the strange–metal phase, however, Nastase points out that the self–energy obeys a different law,

$$\Sigma_{\mathrm{SM}}(\omega) \;\sim\; c\,\omega\log\omega + d\,\omega, \qquad c \in \mathbb{R},\; d \in \mathbb{C}, \tag{3.12}$$

so that the decay rate is *linear* in ω rather than quadratic. The resulting spectral peak near the Fermi surface is wide. A narrow peak corresponds to a long-lived excitation with a well-defined energy, while a broad peak means that the excitation decays quickly. The would-be quasiparticle therefore decays too quickly to support a standard quasiparticle interpretation. One thus has a Fermi surface *without* quasiparticles, in the sense that the excitations are strongly overdamped even at low energies.

These features are naturally interpreted as evidence that the strange–metal state is quantum matter without quasiparticles: its transport properties deviate sharply from Fermi–liquid predictions, spectral probes do not see long–lived quasiparticles, and the relevant relaxation times are expected to be as short as $\tau \sim \hbar/(k_B T)$, in line with the discussion of the bound (3.5)

BKT transitions

Before turning to holography, it is useful to recall another kind of unconventional critical behavior that will reappear later in a holographic setting: the Berezinskii–Kosterlitz–Thouless (BKT) transition. The standard BKT transition appears in two-dimensional systems, such as the XY model, thin superfluids, and superconducting films; see, for example, the review [11].

The BKT transition is different from an ordinary Landau transition. It is not mainly described by a local order parameter becoming small near the critical temperature. Instead, it is associated with the behavior of vortex–antivortex pairs. A characteristic feature of this transition is that physical scales can depend exponentially on the distance from the critical point, rather than by a simple power law.

This distinction will be useful later. In an ordinary second-order transition, quantities often vanish or diverge as powers of the distance from the critical point. In BKT-type behavior, the relevant scale is instead generated exponentially. In this thesis, we will later use the phrase BKT-type scaling for a holographic transition with this exponential form. The detailed holographic mechanism will be introduced after the minimal holographic superconductor has been reviewed.

3.4 Why Holography Is Useful for Transport

Gauge/gravity duality (holography) provides a nonperturbative framework for certain strongly coupled quantum systems [9, 3]. This is useful in the present context because the transport problem is not formulated in terms of individual quasiparticles. Instead, transport is computed from the collective response of the strongly coupled state. For strange metals and quantum–critical phases, its main practical virtues are:

- Finite–density, finite–temperature states in the boundary theory are described by charged black branes in the bulk. Thermodynamic and transport properties of the strongly coupled state are encoded in the classical geometry and fields.

- Transport coefficients are obtained by solving classical bulk equations of motion with infalling boundary conditions at the horizon, which implement causality in the retarded response, and then applying holographic Kubo formulae. No assumption of long–lived quasiparticles is needed: transport emerges from the strongly coupled dynamics of the entire many–body state [9].

In particular, holographic models naturally realize Planckian relaxation and saturation of chaos bounds: the dual black holes exhibit $\tau \sim \hbar/(k_B T)$ and saturate the Lyapunov bound (3.6) [9]. From the boundary perspective, this is precisely the dynamical regime expected for strange metals without quasiparticles and quantum–critical transport.

This is the reason holography is a natural framework for the rest of this thesis: it provides a controlled way to study superconducting instabilities and optical conductivity in a strongly coupled system without assuming a quasiparticle description.

Chapter 4

Holographic Superconductors

In this chapter we review the minimal holographic superconductor construction. We begin from the "phenomenological AdS/CFT" point of view, explaining which bulk ingredients are needed to model a strongly coupled, approximately conformal, charged system that can undergo superconducting/superfluid instabilities. We then present the standard Einstein–Maxwell–scalar model, discuss the mechanism of condensation in terms of an effective mass and BF bounds, and summarize the holographic computation of the optical conductivity. This will be the reference setup for the Weyl–deformed model studied in Chapters 6–8 [4, 12, 3].

4.1 Ingredients of the Holographic Superconductor

The holographic superconductor was put together over several works, with crucial steps by Gubser and by Hartnoll, Herzog and Horowitz [4, 12]. It is a prototypical example of "bottom–up" or phenomenological AdS/CFT: we do not start from a fully specified string theory dual, but instead postulate a bulk effective field theory that has the correct symmetries and field content to model the boundary system of interest.

For the strongly coupled superconductors that motivate AdS/CMT, several qualitative facts guide the construction:

- In a quantum–critical regime the low–energy dynamics are often modeled by an approximately conformal $2+1$-dimensional field theory (a CFT_3). In AdS/CFT such (approximately) scale–invariant regimes are naturally described by asymptotically AdS geometries. Since the relevant electrons live in effectively $2+1$ dimensions in layered materials such as cuprates and organic superconductors, we work in AdS_4, dual to a $d=3$ boundary CFT.

- We are interested in charge transport, so the boundary theory must have a conserved $U(1)$ current J_μ. In the bulk, this is sourced by a gauge field A_μ, which couples as $\int d^3x\, J^\mu A_\mu$ at the boundary.

- We want a superconducting phase, i.e. a phase with spontaneous breaking of (global) $U(1)$ and a nonzero condensate $\langle \mathcal{O} \rangle$. The operator $\mathcal{O}$ couples to a bulk field ψ. For an s-wave superconductor (zero angular momentum on the boundary), the simplest choice is a charged scalar ψ ($s = 0$). More exotic symmetries (e.g. p-wave, d-wave) can be modeled by vector or tensor fields in the bulk, but we will restrict to the scalar case.

- Finally, the boundary theory will be at finite temperature and finite charge density. In holography this requires a black hole (or black brane) in the bulk and a nonzero temporal component A_t of the gauge field.

Putting these ingredients together leads naturally to an Einstein–Maxwell theory in AdS_4 coupled to a charged scalar field. The superconducting phase will correspond to a bulk black hole with "scalar hair", i.e. a solution with $\psi(r) \neq 0$ that is thermodynamically preferred below some critical temperature T_c.

4.2 Minimal Einstein–Maxwell–Scalar Model

4.2.1 Action, probe limit and BF bound

The minimal holographic superconductor is described by the bulk action [12, 5]

$$S_{\min} = \int d^4x\, \sqrt{-g} \left[\frac{1}{2\kappa^2} \left(R + \frac{6}{L^2} \right) - \frac{1}{4g_F^2} F_{\mu\nu} F^{\mu\nu} - |D\psi|^2 - m^2 |\psi|^2 - V(|\psi|) \right], \tag{4.1}$$

where

$$D_\mu = \nabla_\mu - iqA_\mu, \qquad F_{\mu\nu} = \partial_\mu A_\nu - \partial_\nu A_\mu, \tag{4.2}$$

and $V(|\psi|)$ is a self–interaction potential for the scalar. For simplicity we will mostly set $V = 0$; the mass term $m^2|\psi|^2$ will already be sufficient to capture the basic physics. In the holographic dictionary reviewed in Chapter 2, each bulk field has a direct boundary interpretation. The metric describes the finite-temperature state, the gauge field A_μ is dual to the conserved $U(1)$ current, and the charged scalar ψ is dual to the operator that may condense. Thus the model contains the minimal ingredients needed for a charged system with a superconducting instability.

The cosmological constant $\Lambda = -3/L^2$ fixes AdS_4 as a vacuum. In flat space, stability would require $m^2 \geq 0$; in AdS the situation is different. Because of the curvature, a scalar field in AdS is stable even for slightly negative m^2, as long as the Breitenlohner–Freedman (BF) bound [13] is satisfied:

$$m^2 L^2 \geq -\frac{9}{4} \qquad (\mathrm{AdS}_4 \text{ scalar BF bound}). \tag{4.3}$$

The BF bound is therefore not the statement that the scalar mass must be positive. Rather, it is the lower limit below which the AdS vacuum becomes unstable.

For masses in the window

$$-\frac{9}{4} \leq m^2 L^2 < -\frac{5}{4}, \tag{4.4}$$

both standard and alternative quantizations are allowed, corresponding to two different choices of which coefficient in the near-boundary expansion is viewed as the source, and which as the expectation value of the dual operator.

For the purposes of this thesis, it is useful to distinguish two common ways of describing the normal phase. In the probe approximation, the gauge field and the charged scalar are treated as matter fields propagating on a fixed planar Schwarzschild–AdS_4 black brane. This setup is technically simpler and is often sufficient for qualitative discussions and transport computations. In the backreacted description, the Maxwell field modifies the geometry, and the normal phase is described by a charged planar Reissner–Nordström–AdS_4 black brane with vanishing scalar. This second description is especially useful for finite-density thermodynamics and for the near-horizon IR analysis. Throughout this review we will indicate explicitly which background is being used whenever it matters.

4.2.2 Planar black-brane backgrounds and near-boundary data

We focus on homogeneous, isotropic configurations with planar symmetry,

$$ds^2 = -f(r)\,dt^2 + \frac{dr^2}{f(r)} + r^2\,(dx^2 + dy^2), \qquad A = \phi(r)\,dt, \qquad \psi = \psi(r) \in \mathbb{R}, \tag{4.5}$$

T+this ansatz describes a static and spatially homogeneous black-brane configuration.

Near the AdS boundary $r \to \infty$, the fields behave as

$$\phi(r) = \mu - \frac{\rho}{r} + \cdots , \qquad \psi(r) = \psi_- \, r^{-\Delta_-} + \psi_+ \, r^{-\Delta_+} + \cdots , \tag{4.6}$$

with scaling dimensions

$$\Delta_\pm = \frac{3}{2} \pm \sqrt{\frac{9}{4} + m^2 L^2}. \tag{4.7}$$

In the holographic dictionary, μ and ρ are interpreted as chemical potential and charge density, while ψ_- and ψ_+ are the source and vev of the dual operator $\mathcal{O}$, depending on the choice of quantization. As reviewed in Chapter 2, spontaneous condensation means that the source coefficient is set to zero while the normalizable coefficient is allowed to be nonzero.

In the *normal phase* the scalar vanishes, $\psi(r) = 0$, and the metric–gauge sector solves the Einstein–Maxwell equations. There are two backgrounds that will be useful for us:

- **Neutral Schwarzschild–AdS$_4$ black brane .** If we neglect the backreaction of the gauge field and scalar, the metric is that of a neutral planar Schwarzschild–AdS$_4$ black brane,

  $$f(r) = \frac{r^2}{L^2} - \frac{2M}{r}. \tag{4.8}$$

  In this approximation one may still turn on a nontrivial temporal gauge potential $A_t = \phi(r)$ solving the Maxwell equation on this fixed background, thereby introducing a chemical potential μ and charge density ρ in the boundary theory without modifying the geometry. This is the setup used in the original holographic superconductor [5].

- **Charged Reissner–Nordström–AdS$_4$ black brane.** When the backreaction of the Maxwell field is included, the finite-density normal phase is described by a planar RN–AdS$_4$ black brane,

  $$f(r) = \frac{r^2}{L^2} - \frac{2M}{r} + \frac{Q^2}{4r^2}, \qquad \phi(r) = \mu - \frac{Q}{r}, \tag{4.9}$$

  with the horizon radius r_h defined by $f(r_h) = 0$ and regularity requiring $\phi(r_h) = 0$, which implies $\mu = Q/r_h$. Matching (4.9) to the asymptotics (4.6) identifies $\rho = Q$. The Hawking temperature is

  $$T = \frac{f'(r_h)}{4\pi}. \tag{4.10}$$

This is the background on which the superconducting instability develops when the charged scalar condenses.

It is often convenient to rescale to dimensionless variables by setting $L = 1$ and the horizon radius to unity, $r_h = 1$. For the RN–AdS$_4$ solution this gives

$$f(r) = r^2 - \frac{1}{r}\left(1 + \frac{\rho^2}{4}\right) + \frac{\rho^2}{4r^2}, \qquad \phi(r) = \rho\left(1 - \frac{1}{r}\right), \tag{4.11}$$

with $f(1) = 0$ and temperature

$$T = \frac{f'(1)}{4\pi} = \frac{1}{4\pi}\left(3 - \frac{\rho^2}{4}\right). \tag{4.12}$$

These dimensionless conventions will be used below when discussing the superconducting instability and IR analysis, while the neutral Schwarzschild–AdS$_4$ background will reappear in the discussion of transport.

4.2.3 Effective mass and condensation mechanism

As discussed above, the normal phase can be described either in the probe Schwarzschild–AdS$_4$ approximation or in the backreacted RN–AdS$_4$ background. The effective-mass mechanism can be understood in both cases, while the RN–AdS$_4$ description is especially useful for the near-horizon IR analysis [12, 5].

Starting from (4.1), the scalar equation of motion is

$$(D^2 - m^2)\psi = 0, \tag{4.13}$$

with $D_\mu = \nabla_\mu - iqA_\mu$. On the homogeneous ansatz (4.5) this becomes a radial equation for $\psi(r)$. The key point is that the electric potential affects the scalar as if it changed the scalar mass in the interior of the geometry. It is useful to isolate the terms in the action that are quadratic in ψ:

$$-|D\psi|^2 - m^2|\psi|^2 \longrightarrow -g^{rr}|\partial_r\psi|^2 - \left(m^2 + g^{tt}q^2\phi^2\right)|\psi|^2. \tag{4.14}$$

Thus the scalar behaves as a Klein–Gordon field with a position–dependent effective mass

$$m^2_{\text{eff}}(r) = m^2 + g^{tt}(r)\, q^2\phi^2(r). \tag{4.15}$$

Since $g^{tt} < 0$ outside the horizon, the coupling to the electric potential $\phi(r)$ *lowers* the effective mass relative to m^2:

$$m_{\text{eff}}^2(r) < m^2. \tag{4.16}$$

For sufficiently large charge q or chemical potential μ, this lowering can make the scalar unstable in the interior while it remains stable (above the AdS_4 BF bound) near the boundary. This is the basic bulk mechanism behind the superconducting instability [4].

A particularly transparent picture arises in the extremal limit of the backreacted RN–AdS_4 black brane, whose near–horizon region is $AdS_2 \times \mathbb{R}^2$. There the relevant stability criterion is the AdS_2 BF bound

$$m_{\text{eff}}^2 R_2^2 \geq -\frac{1}{4}, \tag{4.17}$$

with R_2 the AdS_2 radius (for RN–AdS_4, $R_2^2 = L^2/6$). If m_{eff}^2 drops below this bound in some radial interval near the horizon, the $\psi = 0$ solution becomes unstable and a static mode $\psi(r) \neq 0$ develops; the full nonlinear equations then admit a new branch of "hairy" black brane solutions with nonzero scalar profile [5, 3].

Thus the scalar can be stable from the point of view of the asymptotic AdS_4 region, but unstable in the near-horizon AdS_2 region. This is why the superconducting instability can be understood as an infrared effect.

From the boundary point of view, the critical temperature T_c is found by looking for the first static scalar mode that can appear without adding an external source. Near the AdS boundary,

$$\psi(r) = \psi_- \, r^{-\Delta_-} + \psi_+ \, r^{-\Delta_+} + \cdots . \tag{4.18}$$

In standard quantization, ψ_- is the source and ψ_+ is proportional to the condensate. Therefore, spontaneous condensation requires

$$\psi_- = 0. \tag{4.19}$$

With this boundary condition and regularity at the horizon, the scalar equation has a nontrivial solution only at special values of the temperature. The highest such temperature is the critical temperature T_c.

At $T = T_c$, this solution should be understood as the first normalizable profile that can appear without an external source. Its overall size is not fixed at the linear level. The physical condensate is determined only below T_c, where the full nonlinear solution develops scalar hair, and it vanishes continuously as $T \to T_c^-$.

In many applications one chooses $m^2L^2 = -2$, for which $\Delta_- = 1$ and $\Delta_+ = 2$, so both modes are normalizable. One can then define two distinct operators $\mathcal{O}_1$ and $\mathcal{O}_2$ by

$$\psi(r) \sim \frac{\psi_{(1)}}{r} + \frac{\psi_{(2)}}{r^2} + \cdots, \qquad \langle \mathcal{O}_1 \rangle \propto \psi_{(1)}, \qquad \langle \mathcal{O}_2 \rangle \propto \psi_{(2)}, \tag{4.20}$$

and study their condensates as functions of temperature. These correspond to two different source-free boundary conditions, not to two independent condensates turned on simultaneously. Numerically one finds that, for both quantizations and for a range of scalar masses above the AdS_4 BF bound, the condensate vanishes near the transition as

$$\langle \mathcal{O} \rangle \ \propto \ \left(1 - T/T_c\right)^{1/2}, \qquad T \to T_c^-, \tag{4.21}$$

i.e. with the mean–field critical exponent $1/2$ [12, 3]. The value of m^2 (equivalently, the operator dimension) affects the critical temperature and the overall scale of the condensate, but not the fact that the transition in this minimal model is second order with mean–field scaling. On dimensional grounds one finds $T_c \propto \mu$ (or $T_c \propto \sqrt{\rho}$ in the canonical ensemble), in agreement with numerical results [12, 3].

4.3 Transport Properties and Mass Gap

4.3.1 Conductivity from bulk fluctuations

The optical conductivity of the boundary theory is encoded in the response of the current J_x to a small electric field along x. In holography, J_x is dual to the bulk gauge field component A_x, so we study a fluctuation

$$\delta A_x(t, r) = A_x(r)\, e^{-i\omega t}, \qquad k = 0, \tag{4.22}$$

on top of the static black-brane background.

Linearizing the Maxwell equation around the background leads to a second-order ODE for $A_x(r)$. For the neutral Schwarzschild–AdS_4 black brane this equation takes the schematic form

$$A_x''(r) + \mathcal{P}(r)\, A_x'(r) + \mathcal{Q}(r;\omega)\, A_x(r) = 0, \tag{4.23}$$

with known functions $\mathcal{P}$, $\mathcal{Q}$ determined by the metric. Ingoing boundary conditions at the horizon

$$A_x(r) \sim (r - r_h)^{-i\omega/(4\pi T)}, \qquad r \to r_h^+, \tag{4.24}$$

implement causality and select the retarded Green's function.

Near the AdS boundary the fluctuation behaves as

$$A_x(r) = A_x^{(0)} + \frac{A_x^{(1)}}{r} + \cdots . \tag{4.25}$$

The boundary electric field is the time derivative of the source, $E_x = -\partial_t A_x^{(0)} = i\omega A_x^{(0)}$, while the induced current is proportional to the subleading coefficient, $J_x \propto A_x^{(1)}$ (with a proportionality factor fixed by the Maxwell coupling). Ohm's law therefore gives

$$\sigma(\omega) = \frac{J_x}{E_x} = -\frac{i}{\omega}\frac{A_x^{(1)}}{A_x^{(0)}} \qquad \text{(up to an overall normalization)}. \tag{4.26}$$

Thus, the conductivity is obtained by solving one radial fluctuation problem: the leading boundary coefficient gives the applied electric field, while the subleading coefficient gives the induced current. The frequency dependence of $\sigma(\omega)$ is therefore encoded in the radial profile of $A_x(r)$ with ingoing boundary conditions at the horizon.

4.3.2 Superconducting-phase conductivity and gap

In the superconducting phase, the nonzero scalar profile $\psi(r)$ modifies the fluctuation equation (4.23) by adding an effective mass term for A_x proportional to $\psi^2(r)$, as in Refs. [12] and the discussion in Nastase [3, Ch. 37]. This reflects the fact that the condensed charged operator changes the response of the current to an applied electric field. Solving for $A_x(r)$ on the hairy black-brane background and inserting the result into (4.26) yields a characteristic optical response with two key features:

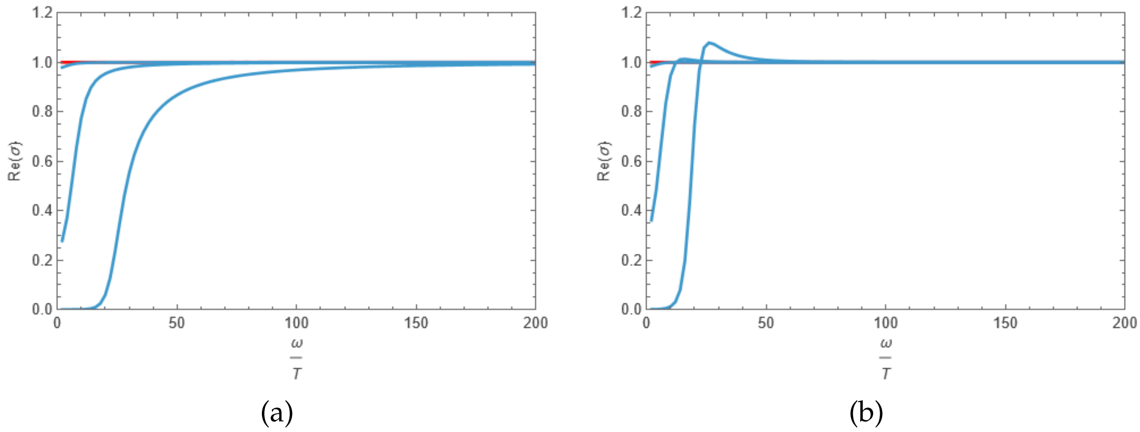

Figura 4.1: **Real part of the optical conductivity.** $\Re\sigma(\omega)$ as a function of ω/T at and below T_c for the minimal holographic superconductor. Panel (a) corresponds to the dimension-one operator, panel (b) to the dimension-two operator; the curve at $T = T_c$ is shown as a red straight line, and the remaining curves correspond to successively lower temperatures. A $\delta(\omega)$ contribution at the origin is present in all cases. *Adapted from* [5].

- **Gap-like (pseudogap) behavior.** The real part $\Re\sigma(\omega)$ is strongly suppressed below a frequency ω_{gap} of order T_c, mimicking the opening of a gap in the charged excitation spectrum, with spectral weight shifted to higher frequencies [12, 3].
- **Delta function at $\omega = 0$.** The imaginary part $\Im\sigma(\omega)$ acquires a pole $\sim n_s/\omega$ as $\omega \to 0$; by the Kramers–Kronig relations this implies $\Re\sigma(\omega) = \pi n_s\,\delta(\omega) + \sigma_{\text{reg}}(\omega)$, signaling infinite DC conductivity in the perfectly homogeneous (translation-invariant) setup limit [12].

Representative numerical results for the real part of the optical conductivity across and below the transition are shown in Fig. 4.1. As T is lowered below T_c, $\Re\sigma(\omega)$ becomes increasingly suppressed at low frequency, approaching a gap-like region, while a $\delta(\omega)$ contribution is present at the origin (not visible in the numerics).

In the simplest probe-limit models with $m^2L^2 = -2$, numerical solutions show that the zero-temperature gap scale ω_{gap} and the critical temperature T_c satisfy a roughly universal ratio $\hbar\omega_{\text{gap}}/k_BT_c \approx 8.4$ in appropriate units, much larger than the weak-coupling BCS value $\hbar\omega_{\text{gap}}/k_BT_c \approx 3.5$ [12, 3].

This is one of the early indications that holographic superconductors capture strong–coupling physics closer in spirit to high-T_c materials than to conventional BCS superconductors.

In summary, the minimal Einstein–Maxwell–scalar model provides a clean holographic realization of an *s*-wave superconductor: the normal phase is described by a planar black brane with a nontrivial temporal gauge potential A_t (Schwarzschild–AdS$_4$ in the probe limit, or RN–AdS$_4$ when backreaction is included). Below a critical temperature T_c the normal phase becomes unstable to developing scalar hair, corresponding to condensation of the dual charged operator. In the backreacted RN description this instability admits a particularly clear IR interpretation in terms of the near-horizon region and an effective-mass/BF-bound criterion. The optical conductivity in the condensed phase exhibits a strongly suppressed low-frequency response together with a zero-frequency δ-peak. In the following chapters we will add a Weyl correction to the gauge sector and study how it modifies this standard holographic superconductor phenomenology.

Chapter 5

Weyl Corrections and Quantum Critical Transport

In this chapter we motivate the specific higher–derivative deformation used in our model,

$$\Delta S_{\text{Weyl}} = \gamma \frac{L^2}{e^2} \int d^4x \sqrt{-g}\, C_{\mu\nu\rho\sigma} F^{\mu\nu} F^{\rho\sigma}, \tag{5.1}$$

from both the gravity/string and condensed–matter perspectives. Our presentation closely follows the discussion of Weyl-type higher-derivative corrections and their transport implications in [7] (see also [3]). We explain how this Weyl coupling arises as a representative four–derivative correction in the bulk, why it naturally breaks the electric–magnetic self–duality of the minimal Einstein–Maxwell theory, and how it modifies quantum–critical transport in the dual CFT. The detailed equations of motion and the probe/small-γ regime will be presented in Chapter 6; here we focus on the motivation and physical interpretation of the Weyl coupling.

5.1 Minimal Holographic Model for Quantum Critical Systems

We are interested in 2+1-dimensional quantum critical systems with a conserved $U(1)$ current. The minimal holographic dual for such a system consists of:

1. a four–dimensional metric $g_{\mu\nu}$, dual to the stress tensor $T_{\mu\nu}$;
2. a negative cosmological constant, fixing the AdS_4 radius L;
3. a bulk $U(1)$ gauge field A_μ, dual to the conserved current J_μ.

At two derivatives, the corresponding effective bulk action has the Einstein–Maxwell form

$$S_0 = \int d^4x\,\sqrt{-g}\left[\frac{1}{2\kappa_4^2}\left(R+\frac{6}{L^2}\right)-\frac{1}{4e^2}F_{\mu\nu}F^{\mu\nu}\right], \tag{5.2}$$

where κ_4 is the four–dimensional gravitational coupling and e is the effective bulk gauge coupling. The cosmological constant has been written in terms of the AdS radius L.

The finite–temperature state of the dual CFT is described by a planar AdS–Schwarzschild black brane. In the radial coordinate $u = r_0/r$, with horizon at $u = 1$ and boundary at $u \to 0$, the metric can be written as

$$ds^2 = \frac{L^2}{u^2}\left(-f(u)\,dt^2 + d\vec{x}^2 + \frac{du^2}{f(u)}\right), \qquad f(u) = 1-u^3, \tag{5.3}$$

and the Hawking temperature is

$$T = \frac{3}{4\pi}\frac{1}{u_h L} = \frac{3r_0}{4\pi L^2}. \tag{5.4}$$

In the neutral phase the background gauge field vanishes, $A_\mu = 0$, and the geometry (5.3) is a solution of the Einstein equations following from (5.2).

The action (5.2) is also the universal two–derivative truncation of many top–down constructions. For example, the ABJM theory in 2+1 dimensions admits a gravity dual in M–theory or type IIA; upon compactification and truncation, one obtains an effective Einstein–Maxwell sector of the form (5.2), with A_μ dual to a particular global $U(1)$ current. In this top–down setting, κ_4 and e are determined by microscopic data such as the rank N and the 't Hooft coupling λ, but for most of the discussion we treat them as effective couplings.

5.2 Higher–Derivative Corrections and the Weyl Term

5.2.1 Effective field theory and four–derivative operators

From the perspective of string or M–theory, (5.2) is only the leading term in a low–energy expansion. At higher orders in α' (or in the inverse AdS curvature scale measured in string units), one expects an infinite tower of higher–derivative corrections, schematically of the form

$$S_{\text{eff}} = S_0 + S_{\text{HD}}, \qquad S_{\text{HD}} = \int d^4x \sqrt{-g}\, \mathcal{L}_{\text{HD}}\big(R_{\mu\nu\rho\sigma}, F_{\mu\nu}, \nabla_\mu\big). \tag{5.5}$$

At this stage the purpose is not to keep all possible higher-derivative terms. Rather, we want to identify which correction can affect the current two-point function, and therefore the optical conductivity, in the simplest controlled way. Restricting to parity–even terms and focusing on corrections that involve the gauge field, the most general four–derivative Lagrangian density can be written, up to integration by parts and Bianchi identities, as a linear combination of operators such as

$$\begin{aligned}\mathcal{L}_{\text{4der}} = {} & \alpha_1 R^2 + \alpha_2 R_{\mu\nu}R^{\mu\nu} + \alpha_3\big(F^2\big)^2 + \alpha_4 F^4 + \alpha_5 \nabla^\mu F_{\mu\nu}\, \nabla^\rho F_\rho{}^\nu + \alpha_6 R_{\mu\nu\rho\sigma}F^{\mu\nu}F^{\rho\sigma} \\ & + \alpha_7 R^{\mu\nu}F_{\mu\rho}F_\nu{}^\rho + \alpha_8 RF^2.\end{aligned} \tag{5.6}$$

where $F^2 \equiv F_{\mu\nu}F^{\mu\nu}$, and the omitted terms involve higher derivatives or different index contractions. The coefficients α_i are (in principle computable) functions of the microscopic CFT data.

Not all four–derivative operators are equally relevant for the transport properties we care about. Focusing on linear response of the charge current at zero spatial momentum, several observations simplify the problem:

- Pure curvature–squared invariants (without $F_{\mu\nu}$) only modify the stress–tensor correlators, not the current–current correlator at leading order.
- Operators with four field strengths, such as $(F^2)^2$ or F^4, first affect four–point functions of J_μ; they do not enter the two–point function at linear order in fluctuations around $A_\mu = 0$ and hence do not change the conductivity at zero density.
- Derivative terms like $(\nabla F)^2$ generically produce higher–order equations of motion for A_μ and lead to ghosts in the spectrum, which indicates nonunitarity in the dual CFT.
- Certain combinations of RF^2 and $R_{\mu\nu}F^{\mu\rho}F^\nu{}_\rho$ simply renormalize the overall Maxwell coupling and therefore change the normalization of the conductivity without altering its frequency dependence.

Thus, most four-derivative terms either do not affect the conductivity at linear order, change only an overall normalization, or introduce unwanted higher-order dynamics. After imposing these requirements and using field redefinitions to remove redundant operators, one is naturally led to a single nontrivial four–derivative interaction that can affect linear charge transport in a controlled way: a contraction of two field strengths with the Weyl tensor $C_{\mu\nu\rho\sigma}$. We therefore adopt the gauge–field sector

$$S_{\text{gauge}} = \int d^4x \sqrt{-g} \left[-\frac{1}{4e^2} F_{\mu\nu} F^{\mu\nu} + \gamma \frac{L^2}{e^2} C_{\mu\nu\rho\sigma} F^{\mu\nu} F^{\rho\sigma} \right], \tag{5.7}$$

where we have factored out L^2 so that γ is dimensionless. In a strict top–down embedding γ would be small and fixed (e.g. scaling like a negative power of the 't Hooft coupling), but here we take a bottom–up viewpoint and treat γ as a tunable parameter, subject only to consistency bounds discussed below.

5.2.2 Why the Weyl tensor is special

It is important that the curvature tensor appearing in (5.7) be chosen to be the Weyl tensor,

$$C_{\mu\nu\rho\sigma} = R_{\mu\nu\rho\sigma} - \frac{2}{d-2} \left(g_{\mu[\rho} R_{\sigma]\nu} - g_{\nu[\rho} R_{\sigma]\mu} \right) + \frac{2}{(d-1)(d-2)} R\, g_{\mu[\rho} g_{\sigma]\nu}, \tag{5.8}$$

with $d = 4$ in our case. It differs from the Riemann tensor by traces chosen such that:

$$C_{\mu\nu\rho\sigma} = 0 \quad \text{in pure AdS}_4, \tag{5.9}$$

whereas $R_{\mu\nu\rho\sigma}$ is nonzero and constant. This property is useful because it makes the correction sensitive to deviations from pure AdS, rather than changing the UV CFT vacuum itself.

This has several consequences:

1. **AdS_4 remains an exact solution.** Since $C_{\mu\nu\rho\sigma} = 0$ on AdS_4, the Weyl term does not contribute to the background equations of motion, and the AdS vacuum remains unchanged. In particular, the vacuum two–point functions $\langle JJ \rangle_0$ and $\langle TT \rangle_0$ are independent of γ.

2. **Neutral AdS black branes are unchanged at leading order.** For the neutral black brane (5.3), the background gauge field vanishes. Therefore the Weyl term does not change the background solution at the level considered here. In the probe/small-γ regime, we keep the metric fixed and treat the Weyl

interaction as a deformation of the gauge-field fluctuations. This keeps the geometry analytically tractable while still allowing γ to affect charge transport.

3. **The UV fixed point is preserved.** Near the boundary, the geometry approaches AdS_4 and $C_{\mu\nu\rho\sigma} \to 0$. Therefore the high–frequency (UV) behavior of correlation functions is unaffected by γ, and we remain at the same conformal fixed point. The Weyl term only modifies the response in regions with nontrivial curvature, such as near the horizon at finite temperature.

4. **It directly deforms current correlators.** Unlike pure curvature–squared terms, the Weyl coupling appears already in the two–point function of the current at finite temperature. As a result, it modifies the conductivity at order γ, and will allow us to break the trivial frequency independence of the self–dual Einstein–Maxwell theory.

Varying (5.7) with respect to A_μ yields the modified Maxwell equations

$$\nabla_\mu \left(F^{\mu\nu} - 4\gamma L^2 C^{\mu\nu\rho\sigma} F_{\rho\sigma} \right) = J^\nu_{\text{matter}}, \tag{5.10}$$

where J^ν_{matter} denotes the current sourced by charged matter fields (e.g. the scalar condensate in the superconducting phase). In the normal phase $J^\nu_{\text{matter}} = 0$, and the entire linear response of the conserved boundary current is encoded in (6.6).

5.3 Self–Dual Einstein–Maxwell and the Need for Corrections

5.3.1 Electric–magnetic self–duality and constant conductivity

The reason the minimal Maxwell theory is so restrictive is that electric and magnetic responses are not independent in four bulk dimensions. The two–derivative Einstein–Maxwell theory (5.2) in four dimensions enjoys an electric–magnetic (EM) self–duality: in vacuum the equations of motion and Bianchi identity for F are invariant under rotations in the two–dimensional space spanned by F and its Hodge dual $*F$. On an AdS_4 black brane background this duality has a sharp holographic consequence [14, 7]: at zero spatial momentum the optical conductivity of the dual CFT is exactly frequency–independent,

$$\sigma(\omega) = \sigma_\star = \frac{1}{e^2}, \tag{5.11}$$

for all ω/T.

From the condensed–matter perspective this result provides a simple model for "perfect quantum fluids" near 2+1-dimensional quantum critical points. Such systems are expected to relax back to local equilibrium in a time $\tau \sim \hbar/(k_B T)$, the shortest allowed by quantum mechanics, and to exhibit transport coefficients of order $\sigma \sim e^2/h$ and $\eta \sim \hbar s/k_B$. Some experimental systems indeed show only mild frequency dependence of σ over the window $\hbar\omega \sim k_B T$.

However, real quantum critical systems in two spatial dimensions often display nontrivial ω/T dependence and particle–vortex asymmetries that cannot be captured by the self–dual Einstein–Maxwell theory. We would like to explore such more general transport behaviors while *staying* at a conformal fixed point, i.e. without turning on extra scalar operators with nontrivial profiles. The Weyl interaction (5.7) is the minimal higher–derivative correction that accomplishes this.

5.3.2 Breaking self–duality with the Weyl coupling

It is useful to rewrite (6.6) in terms of a tensor $X^{\mu\nu}{}_{\rho\sigma}$ acting on two–forms:

$$X^{\mu\nu}{}_{\rho\sigma} = \frac{1}{2}\left(\delta^\mu_\rho \delta^\nu_\sigma - \delta^\mu_\sigma \delta^\nu_\rho\right) - 4\gamma L^2 C^{\mu\nu}{}_{\rho\sigma}, \tag{5.12}$$

so that

$$\nabla_\mu \left(X^{\mu\nu}{}_{\rho\sigma} F^{\rho\sigma}\right) = 0. \tag{5.13}$$

For pure Maxwell theory $\gamma = 0$, X is proportional to the identity on two–forms, and EM duality acts as a simple rotation mixing F and $*F$. For $\gamma \neq 0$, X acquires nontrivial structure determined by the Weyl curvature, and the dual of the equation of motion is no longer equivalent to the Bianchi identity. In other words, EM self–duality is broken, and the strong constraint (5.11) on the conductivity is lifted.

On the neutral AdS_4 black brane background (5.3), solving the fluctuation equations following from (6.6) with infalling boundary conditions at the horizon, one finds a frequency–dependent conductivity $\sigma(\omega/T;\gamma)$ with the following general features [7]:

- The high–frequency limit is unchanged, $\sigma(\omega \to \infty) = \sigma_\star$, because near the boundary $C_{\mu\nu\rho\sigma} \to 0$ and the Weyl correction becomes irrelevant.
- The DC limit is modified as

$$\frac{\sigma(\omega = 0)}{\sigma(\omega = \infty)} = 1 + 4\gamma. \tag{5.14}$$

  Thus $\gamma > 0$ (respectively $\gamma < 0$) enhances (respectively suppresses) the DC conductivity relative to the high–frequency value.

- The full $\sigma(\omega/T)$ develops a nontrivial, generally nonmonotonic frequency dependence, which will be important when we discuss the physical interpretation of γ.

5.4 Causality Bounds and CFT Interpretation

5.4.1 Consistency constraints on γ

From a purely bottom–up perspective, the Weyl coupling γ could be an arbitrary dimensionless parameter. However, once we demand that the holographic dual be a sensible CFT, various consistency conditions constrain its allowed range.

In particular, analyses of the Einstein–Maxwell–Weyl system in AdS_4 have imposed *micro–causality* of current correlators, positivity of energy flux, and the absence of ghost–like modes in the higher–derivative sector. These requirements translate into bounds on γ in the dual CFT [7]. For the neutral AdS_4 black brane backgrounds relevant here, they imply that γ must lie in a narrow window around zero,[1]

$$-\frac{1}{12} \leq \gamma \leq \frac{1}{12}. \tag{5.15}$$

In this thesis we simply adopt this range and work well inside it, often perturbatively in $|\gamma| \ll 1$, without attempting to re–derive these bounds.

Combining (5.15) with the DC/UV ratio $\sigma(0)/\sigma(\infty) = 1 + 4\gamma$ from eq. (5.14), we see that

$$\frac{\sigma(0)}{\sigma(\infty)} \in \left[\tfrac{2}{3}, \tfrac{4}{3}\right]. \tag{5.16}$$

Thus, even when self–duality is broken as much as allowed by the consistency conditions above, the DC conductivity still differs from the self–dual value only by

[1] In particular, see the discussion around eq. (34) of Myers et al. [7].

an $\mathcal{O}(1)$ factor. This is in sharp contrast with weak–coupling approaches, where $\sigma(0)/\sigma(\infty)$ can become parametrically large in suitable limits.

5.5 Quantum Critical Transport and Particle–Vortex Duality

5.5.1 Shape of $\sigma(\omega)$ and the sign of γ

The detailed analysis of $\sigma(\omega/T;\gamma)$ in the neutral AdS_4 black brane shows that the sign of γ selects qualitatively different regimes for quantum critical transport:

- For $\gamma > 0$, the conductivity has a *particle–like* profile. There is a Drude–like peak at small ω, smoothly connecting to the constant plateau $\sigma(\omega \to \infty) = \sigma_\star$ at large ω. This resembles the behavior expected from a Boltzmann transport theory of interacting charged quasiparticles.
- For $\gamma < 0$, it is instead the *resistivity* $1/\sigma(\omega)$ that develops a Drude–like peak at low frequencies. In this case a more natural interpretation is in terms of a dual description where vortices (rather than particles) undergo scattering processes that determine the long–time response.

In 2+1 dimensions, particle–vortex duality maps the conductivity of a particle description to the resistivity of a vortex description. The Weyl coupling therefore provides a simple holographic knob that moves the system between particle–dominated and vortex–dominated transport regimes near a quantum critical point.

5.5.2 Bulk EM duality and boundary particle–vortex duality

In the bulk, EM duality can still be defined for the Weyl–modified theory, but it no longer acts as a symmetry. One can construct an EM dual action with its own effective coupling and corresponding conductivity $\hat{\sigma}(\omega)$. At zero and infinite frequency the original and dual conductivities are approximately inverse to each other, as expected from particle–vortex duality. Away from these limits the relation is more complicated, reflecting the breakdown of exact self–duality once $\gamma \neq 0$.

Holographically, this picture ties together:

- the loss of EM self–duality in the bulk due to the Weyl term;

- the appearance of particle–vortex asymmetry in the boundary CFT;
- and the interpretation of γ as a parameter controlling which set of excitations (particles or vortices) provides a more natural kinetic description of transport.

5.6 Top–Down Motivation: ABJM and Landau–Ginzburg Physics

The previous sections motivated the Weyl coupling from the point of view of effective transport. We now briefly explain why such a correction is also natural from a top-down perspective. This discussion is not needed for the later computations, but it provides additional motivation for treating the Weyl term as a controlled effective deformation.

5.6.1 String corrections in ABJM–like models

In a top–down setting such as the ABJM theory, the four–dimensional action (5.2) arises from dimensional reduction of the full ten– or eleven–dimensional supergravity background [3, Ch. 42]. String corrections generate higher–derivative terms, including those of the schematic form

$$R^2, \qquad RF^2, \qquad R_{\mu\nu\rho\sigma}F^{\mu\nu}F^{\rho\sigma}, \qquad R^nF^2, \quad n \geq 2, \tag{5.17}$$

among many others. At the four–derivative level, these string corrections can be organized into the Weyl interaction (5.7) plus other terms that either renormalize couplings or affect higher–point functions.

The combination (5.7) is particularly convenient because:

- it vanishes in AdS and therefore does not alter the UV fixed point;
- it captures, in a single parameter γ, the leading corrections to charge transport at finite temperature;
- it has a clear CFT interpretation in terms of the extra structure in the three–point function $\langle TJJ \rangle$.

In this sense, the Einstein–Maxwell–Weyl system provides a toy gravity dual to an ABJM–like CFT, where γ encodes the effect of finite 't Hooft coupling and stringy corrections on transport observables.

5.6.2 Effective Landau–Ginzburg description

In many condensed–matter systems, the low–energy physics near a quantum critical point is captured by an effective relativistic Landau–Ginzburg (LG) model for a complex scalar order parameter, possibly coupled to a $U(1)$ gauge field. The microscopic lattice Hamiltonian may be complicated, but the LG theory correctly describes the macroscopic behavior in the scaling regime.

In a holographic context like ABJM, the situation is analogous. The full microscopic theory is a nonabelian large–N CFT, but an effective LG description emerges in appropriate sectors: a particular scalar operator (or set of operators) plays the role of the order parameter, and the $U(1)$ global current is encoded in the bulk gauge field. From the bulk point of view this corresponds to an Einstein–Maxwell–scalar system in AdS_4, possibly supplemented by higher–derivative interactions such as the Weyl term.

The fact that the LG model is abelian while the microscopic CFT has a large nonabelian gauge group is not an obstacle. The LG sector appears as a nontrivial embedding inside the full theory: it corresponds to a consistent truncation of the gravity dual where only a subset of fields (metric, one gauge field, one scalar) are kept active. The Weyl term then captures universal features of how stringy corrections deform transport in this truncated sector, without requiring us to compute the full higher–derivative action of the underlying string background.
In summary, the Weyl term (5.1) provides a simple but rich one–parameter extension of the minimal holographic superconductor. It preserves the UV fixed point while substantially enlarging the space of possible quantum–critical transport behaviors in the IR, and it admits a natural interpretation both from the string–theory (ABJM) side and from the condensed–matter side in terms of particle–vortex duality and nearly perfect quantum fluids. In the next chapters we will make this picture quantitative by analyzing the IR solution and the full optical conductivity in the presence of γ.

Chapter 6

Model Setup

In this chapter we introduce only the bulk ingredients we will actually solve on in the Weyl-corrected holographic superconductor: the Einstein–Maxwell–scalar action with a Weyl coupling, the homogeneous planar ansatz, and the probe/small-γ regime. We show that in the probe/small-γ regime the *geometry*, to the order considered here, coincides with that of the minimal holographic superconductor model, while the Weyl coupling γ deforms the gauge-sector equations.

6.1 Action and Ansatz (with γ)

We consider an Einstein–Maxwell–scalar theory in AdS_4 deformed by a Weyl coupling in the gauge sector:

$$S = \int d^4x\,\sqrt{-g}\left[\frac{1}{2\kappa^2}\left(R+\frac{6}{L^2}\right) - \frac{1}{4g_4^2}F_{\mu\nu}F^{\mu\nu} - |D\psi|^2 - m^2|\psi|^2 + \gamma\frac{L^2}{g_4^2}\,C_{\mu\nu\rho\sigma}F^{\mu\nu}F^{\rho\sigma}\right], \tag{6.1}$$

where $D_\mu = \nabla_\mu - iqA_\mu$, $F_{\mu\nu} = \partial_\mu A_\nu - \partial_\nu A_\mu$, and $C_{\mu\nu\rho\sigma}$ is the Weyl tensor. We use mostly-plus signature $(-,+,+,+)$, AdS radius L, and $2\kappa^2 = 16\pi G$. In these conventions γ is dimensionless.

We restrict to homogeneous, isotropic states with the standard planar black-brane ansatz

$$ds^2 = -f(r)\,dt^2 + \frac{dr^2}{f(r)} + r^2\,(dx^2+dy^2), \qquad A = A_t(r)\,dt, \qquad \psi = \psi(r) \in \mathbb{R}, \tag{6.2}$$

where, starting from a complex static homogeneous scalar $\psi(r)$, the r-component of Maxwell's equation implies that its phase is constant, so without loss of generality ψ may be taken to be real. Translational invariance in the (x,y)-directions is imposed throughout this chapter.

Near the AdS boundary $r \to \infty$, the fields admit the asymptotic expansions

$$A_t(r) = \mu - \frac{\rho}{r} + \cdots, \qquad \psi(r) = \psi_- \, r^{-\Delta_-} + \psi_+ \, r^{-\Delta_+} + \cdots, \tag{6.3}$$

with scaling dimensions

$$\Delta_\pm = \frac{3}{2} \pm \sqrt{\frac{9}{4} + m^2 L^2}. \tag{6.4}$$

We choose standard or alternative quantization depending on m^2L^2, with both options available above the AdS_4 Breitenlohner–Freedman bound $m^2L^2 \geq -9/4$. The coefficients μ and ρ are interpreted as chemical potential and charge density, respectively, as reviewed in Chapter 4.

6.2 Equations of Motion and Probe/Small-γ Regime

Varying the action (6.1) with respect to $g_{\mu\nu}$, A_μ, and ψ yields the equations of motion

$$G_{\mu\nu} - \frac{3}{L^2} g_{\mu\nu} = \kappa^2 \, T_{\mu\nu}[F, \psi] + \kappa^2 \, \gamma \, \Theta_{\mu\nu}[C, F], \tag{6.5}$$

$$\nabla_\mu \Big(F^{\mu\nu} - 4\gamma L^2 \, C^{\mu\nu\rho\sigma} F_{\rho\sigma} \Big) = g_4^2 \, J^\nu(\psi),, \qquad J^\nu(\psi) = iq \big[\psi^* D^\nu \psi - (D^\nu \psi)^* \psi \big], \tag{6.6}$$

$$(D^2 - m^2) \, \psi = 0. \tag{6.7}$$

Here $T_{\mu\nu}$ is the standard Maxwell–scalar stress tensor, while $\Theta_{\mu\nu}$ arises from the Weyl coupling. Equation (6.6) shows explicitly that γ deforms the gauge equations by a Weyl-tensor contraction.

It is useful to distinguish two small parameters:

- κ^2, which controls *gravitational backreaction* of the matter sector on the geometry;
- γ, which controls *higher-derivative corrections* in the gauge sector.

In this thesis we work in a regime where both are small in a controlled sense.

Probe limit and small-γ. We take the *probe limit* $\kappa^2 \to 0$ (or, more generally, $\kappa^2 \ll 1$) and retain terms up to linear order in γ. In this scaling, all matter backreaction terms on the metric—including the Weyl contribution—enter the right-hand side of (6.5) at order $\mathcal{O}(\kappa^2)$. Consequently, metric corrections induced by the matter fields and by the Weyl term are of order $\mathcal{O}(\kappa^2)$ and $\mathcal{O}(\kappa^2\gamma)$, and are consistently neglected.

Therefore, in the regime of interest we take the $\gamma = 0$ charged black-brane solution as the fixed background geometry and neglect the $\mathcal{O}(\kappa^2)$ backreaction of the scalar sector together with the $\mathcal{O}(\gamma)$ corrections to the metric. The **gauge sector**, on the other hand, obeys the modified Maxwell equation (6.6); for small γ one may view the solutions as controlled deformations of the $\gamma = 0$ Maxwell profiles on the chosen background. In this chapter we will not require the explicit $\mathcal{O}(\gamma)$ corrections to $A_t(r)$; only the existence of such deformations and the fact that the geometry remains fixed will be important.

6.3 Conventions and Dimensionless Units

For conceptual clarity in the previous sections, we have kept the AdS radius L and the horizon radius r_h explicit. However, for the IR analysis and transport calculations it is convenient to adopt dimensionless units in which these reference scales are set to one.

Dimensionless prescription. From Chapter 7 onward we work with

$$L = 1, \qquad r_h = 1, \tag{6.8}$$

so that all radial coordinates and thermodynamic quantities are implicitly measured in units of the AdS radius and the horizon radius. In these units, the RN–AdS_4 metric and thermodynamic quantities simplify accordingly, and the near-horizon AdS_2 geometry will be particularly transparent.

When necessary, physical units can be restored by reinserting appropriate powers of L and r_h, or equivalently by using μ or T as a reference scale. Unless explicitly stated otherwise, all formulas in Chapters 7 and 8 are written in these dimensionless units.

Chapter 7

IR Analysis and BKT Scaling

In this chapter we analyze the infrared (IR) physics of the Weyl-corrected holographic superconductor in the normal phase, focusing on the emergence of a Berezinskii–Kosterlitz–Thouless (BKT) type transition. We zoom into the near-horizon $AdS_2 \times \mathbb{R}^2$ region of the extremal planar RN–AdS_4 black brane, compute how the Weyl coupling γ renormalizes the IR electric parameter $e_d(\gamma)$, derive the IR scaling exponent $\nu(\gamma)$, and show how violation of the AdS_2 BF bound leads to an Efimov-like tower of states and an exponentially small critical temperature

$$T_c(\gamma) \sim \Lambda \exp\left[-\frac{\pi}{\sqrt{-\nu(\gamma)^2}}\right]$$

characteristic of BKT scaling.

Throughout this chapter we work with the charged planar RN–AdS_4 black brane at finite density, in the dimensionless units $L = 1$, $r_h = 1$ introduced in Section 6.3 of Chapter 6. We stay in the *normal phase* with $\psi = 0$ and consider translationally invariant scalar perturbations ($k_x = k_y = 0$), which are the modes that first become unstable and trigger the superconducting transition.

7.1 Near-horizon AdS_2 Geometry

In the normal phase, the background is the planar RN–AdS_4 black brane with metric

$$ds^2 = -f(r)\,dt^2 + \frac{dr^2}{f(r)} + r^2\,(dx^2 + dy^2), \tag{7.1}$$

and a purely electric gauge field $A_t(r)$ as in Chapter 4. At zero temperature (extremality) the blackening factor $f(r)$ has a *double zero* at the horizon $r = r_h = 1$, and near the horizon we can write

$$f(r) \approx 6\,(r-1)^2 + \cdots, \qquad (r \to 1), \tag{7.2}$$

in the units $L = 1$, $r_h = 1$. Substituting (7.2) into (7.1) gives the near-horizon metric

$$ds^2 \approx -6(r-1)^2 dt^2 + \frac{dr^2}{6(r-1)^2} + d\vec{x}_2^2, \qquad d\vec{x}_2^2 \equiv dx^2 + dy^2. \tag{7.3}$$

To exhibit the AdS_2 structure more clearly and avoid confusion with the charge density ρ, we introduce a new radial coordinate ϱ defined by

$$\varrho = 6(r-1), \qquad d\varrho = 6\,dr. \tag{7.4}$$

Then (7.3) becomes

$$ds^2 \approx -\frac{\varrho^2}{6}\,dt^2 + \frac{d\varrho^2}{6\varrho^2} + d\vec{x}_2^2 = \frac{1}{6}\left(-\varrho^2 dt^2 + \frac{d\varrho^2}{\varrho^2}\right) + d\vec{x}_2^2. \tag{7.5}$$

Now define the AdS_2 radial coordinate

$$\zeta = \frac{1}{\varrho}, \qquad d\zeta = -\frac{d\varrho}{\varrho^2}, \qquad d\zeta^2 = \frac{d\varrho^2}{\varrho^4}, \tag{7.6}$$

and keep the time coordinate unchanged, $\tau = t$. Using $\varrho = 1/\zeta$, we find

$$-\varrho^2 dt^2 + \frac{d\varrho^2}{\varrho^2} = -\frac{1}{\zeta^2}d\tau^2 + \frac{1}{\zeta^2}d\zeta^2 = \frac{1}{\zeta^2}\left(-d\tau^2 + d\zeta^2\right). \tag{7.7}$$

Thus (7.5) becomes

$$ds^2 \approx \frac{1}{6\zeta^2}\left(-d\tau^2 + d\zeta^2\right) + d\vec{x}_2^2. \tag{7.8}$$

This is $AdS_2 \times \mathbb{R}^2$ in Poincaré coordinates with

$$R_2^2 = \frac{1}{6}, \tag{7.9}$$

and AdS_2 boundary at $\zeta \to 0$.

In what follows we will focus on this AdS_2 factor,

$$ds^2_{AdS_2} = \frac{R_2^2}{\zeta^2}\left(-d\tau^2 + d\zeta^2\right), \qquad R_2^2 = \frac{1}{6}, \tag{7.10}$$

and treat the $\mathbb{R}^2$ directions as spectators.

7.2 IR Gauge Field and Definition of e_d

7.2.1 Regular gauge near the horizon

In the normal phase the background gauge field has only a time component, $A_\mu = A_t(r)\,\delta^t_\mu$, and we impose the regularity condition that A_t vanishes at the extremal horizon,

$$A_t(r_h = 1) = 0. \tag{7.11}$$

Expanding near the horizon,

$$A_t(r) = A_t'(r_h)\,(r - r_h) + \cdots = A_t'(1)\,(r-1) + \cdots, \tag{7.12}$$

and using $A_r = 0$.

In the AdS_2 chart, the time coordinate is $\tau = t$, and the radial coordinate is ζ defined by (7.6) and (7.4), so that

$$r - 1 = \frac{\varrho}{6} = \frac{1}{6\zeta}. \tag{7.13}$$

Thus the AdS_2 time component of the gauge field is

$$A_\tau(\zeta) = \frac{dt}{d\tau}\,A_t(r(\zeta)) = A_t(r(\zeta)) = A_t'(1)\,(r-1) = \frac{A_t'(1)}{6}\,\frac{1}{\zeta} = \frac{\phi'(1)}{6}\,\frac{1}{\zeta}, \tag{7.14}$$

where we have written $A_t'(1) \equiv \phi'(1)$ for brevity.

On the other hand, in the AdS_2 description it is standard to parametrize a constant electric field background by

$$A_\tau(\zeta) = \frac{e_d}{\zeta}, \tag{7.15}$$

with a dimensionless parameter e_d that measures the IR electric field strength [15]. Comparing (7.14) and (7.15), we obtain the general relation

$$e_d = \frac{1}{6}\,\phi'(1) = R_2^2\,\phi'(1), \tag{7.16}$$

since $R_2^2 = 1/6$. This is the definition of e_d that we will use throughout: it is the near-horizon electric field in AdS_2 units.

7.2.2 Weyl-corrected Maxwell equation and $e_d(\gamma)$

We now determine how the Weyl coupling γ modifies the IR electric parameter e_d. In the normal phase, where $\psi = 0$, the Weyl-modified Maxwell equation (6.6) from Chapter 6 reduces to

$$\nabla_\mu \left(F^{\mu\nu} - 4\gamma \, C^{\mu\nu\rho\sigma} F_{\rho\sigma} \right) = 0. \tag{7.17}$$

For a static, homogeneous electric ansatz $A_\mu = \phi(r)\, \delta^t_\mu$, the only nontrivial component is the $\nu = t$ equation, which can be written as

$$\partial_r \left(\sqrt{-g} \left[F^{rt} - 4\gamma \, C^{rt\rho\sigma} F_{\rho\sigma} \right] \right) = 0. \tag{7.18}$$

With our ansatz, the only nonzero component of $F_{\mu\nu}$ is $F_{rt} = \partial_r A_t = \phi'(r)$, so

$$F^{rt} = g^{rr} g^{tt} F_{rt} = g^{rr} g^{tt} \phi'(r), \tag{7.19}$$

and the Weyl contraction reduces to

$$C^{rt\rho\sigma} F_{\rho\sigma} = C^{rtrt} F_{rt} + C^{rttr} F_{tr} = C^{rtrt} \phi'(r) + (-C^{rtrt})(-\phi'(r)) = 2\, C^{rtrt}\, \phi'(r). \tag{7.20}$$

Therefore

$$F^{rt} - 4\gamma \, C^{rt\rho\sigma} F_{\rho\sigma} = \left(g^{rr} g^{tt} - 8\gamma C^{rtrt} \right) \phi'(r), \tag{7.21}$$

and (7.18) becomes

$$\partial_r \left(\sqrt{-g} \left[g^{rr} g^{tt} - 8\gamma \, C^{rtrt} \right] \phi'(r) \right) = 0. \tag{7.22}$$

This implies

$$\sqrt{-g} \left[g^{rr} g^{tt} - 8\gamma \, C^{rtrt} \right] \phi'(r) = \text{const}. \tag{7.23}$$

In the UV region, where the Weyl tensor vanishes and the metric is asymptotic to AdS_4, the gauge field behaves as

$$\phi(r) = \mu - \frac{\rho}{r} + \cdots, \tag{7.24}$$

so that ρ is the charge density of the dual field theory. In the absence of the Weyl term, the radial electric flux is proportional to $-\rho$. We therefore fix the integration constant in (7.23) as

$$\sqrt{-g}\,\left[g^{rr}g^{tt} - 8\gamma\, C^{rtrt}\right] \phi'(r) = -\rho. \tag{7.25}$$

Near the extremal horizon $r = 1$, the metric (7.3) implies (in the units $L = 1$, $r_h = 1$)

$$\sqrt{-g}\Big|_{r=1} = 1, \qquad g^{rr}g^{tt}\Big|_{r=1} = -1. \tag{7.26}$$

For the extremal planar RN–AdS$_4$ solution in this normalization, the relevant Weyl-tensor component evaluated at the horizon is

$$C_{rtrt}(r_h) = 2, \qquad C^{rtrt}(r_h) = (g^{rr}g^{tt})^2 C_{rtrt}(r_h) = 2. \tag{7.27}$$

Substituting into (7.25) at $r = 1$, we find

$$(-1 - 16\gamma)\,\phi'(1) = -\rho, \tag{7.28}$$

so that the near-horizon electric field is

$$\phi'(1) = \frac{\rho}{1 + 16\gamma}. \tag{7.29}$$

For $\gamma = 0$, this correctly reproduces the minimal RN–AdS$_4$ result, $\phi'(1) = \rho$, consistent with $A_t(r) = \mu - \rho/r$.

Combining (7.16) and (7.29), we obtain the IR electric parameter as a function of the Weyl coupling:

$$e_d(\gamma) = \frac{1}{6}\,\phi'(1) = \frac{\rho}{6(1 + 16\gamma)}. \tag{7.30}$$

In particular, for $\gamma = 0$,

$$e_d(0) = \frac{\rho}{6}. \tag{7.31}$$

To linear order in γ we can expand

$$e_d(\gamma) = \frac{\rho}{6}\,\frac{1}{1 + 16\gamma} \simeq \frac{\rho}{6}\left(1 - 16\gamma + \mathcal{O}(\gamma^2)\right). \tag{7.32}$$

Thus a positive Weyl coupling $\gamma > 0$ reduces the magnitude of the IR electric parameter in this convention; this will directly affect the IR scaling exponent.

7.3 Scalar IR Scaling and AdS_2 BF Bound

7.3.1 Scalar in AdS_2 with electric field

We now consider the charged scalar in the AdS_2 region following the analysis of Faulkner, Liu, McGreevy, and Vegh [15]. The quadratic scalar action in the AdS_2 background is

$$S_{\mathrm{IR}} = -\int d^2x\,\sqrt{-g}\,\left[(D^\alpha\phi)^* D_\alpha\phi + m^2\phi^*\phi\right], \tag{7.33}$$

with

$$D_\alpha = \partial_\alpha - iqA_\alpha, \tag{7.34}$$

and the AdS_2 metric and gauge field given by

$$ds^2 = \frac{R_2^2}{\zeta^2}\left(-d\tau^2 + d\zeta^2\right), \qquad A_\tau(\zeta) = \frac{e_d}{\zeta}, \qquad A_\zeta = 0, \tag{7.35}$$

with $R_2^2 = 1/6$ and e_d given by (7.30).

Writing

$$\phi(\tau,\zeta) = e^{-i\omega\tau}\,\phi(\omega,\zeta), \tag{7.36}$$

the scalar wave equation can be cast in Schrödinger form

$$-\partial_\zeta^2\phi(\omega,\zeta) + V(\zeta)\,\phi(\omega,\zeta) = 0, \tag{7.37}$$

with effective potential

$$V(\zeta) = \frac{m^2R_2^2}{\zeta^2} - \left(\omega + \frac{qe_d}{\zeta}\right)^2. \tag{7.38}$$

To extract the IR scaling dimension, we study the behavior near the AdS_2 boundary $\zeta \to 0$, where the potential is dominated by the ζ^{-2} terms and one can neglect ω compared to qe_d/ζ. The general solution in this limit behaves as [15]

$$\phi(\omega,\zeta) = A(\omega)\,\zeta^{\frac{1}{2}-\nu}\,(1+\mathcal{O}(\zeta)) + B(\omega)\,\zeta^{\frac{1}{2}+\nu}\,(1+\mathcal{O}(\zeta))\,, \qquad \zeta \to 0, \tag{7.39}$$

with

$$\nu(\gamma) = \sqrt{m^2R_2^2 - q^2e_d(\gamma)^2 + \frac{1}{4} - i\epsilon}, \tag{7.40}$$

and $e_d(\gamma)$ given by (7.30). The small $-i\epsilon$ picks the correct branch of the square root for the retarded Green's function.

The conformal dimension of the dual IR operator $\mathcal{O}_{\mathrm{IR}}$ living in the emergent CFT_1 is then

$$\delta_{\mathrm{IR}}(\gamma) = \frac{1}{2} + \nu(\gamma). \tag{7.41}$$

Note that δ_{IR} depends on both the bulk mass m and the charge q via the combination $m^2 R_2^2 - q^2 e_d^2$, and thus is sensitive to the Weyl coupling γ through $e_d(\gamma)$.

Using $R_2^2 = 1/6$ and (7.30), the exponent can be written explicitly as

$$\nu(\gamma) = \sqrt{\frac{m^2}{6} - q^2\left(\frac{\rho}{6(1+16\gamma)}\right)^2 + \frac{1}{4} - i\epsilon}. \tag{7.42}$$

7.3.2 AdS_2 BF bound and critical surface

In AdS_2, the Breitenlohner–Freedman bound for a charged scalar with effective mass m_{eff}^2 and electric coupling qe_d is

$$m_{\mathrm{eff}}^2 R_2^2 \geq -\frac{1}{4}, \qquad m_{\mathrm{eff}}^2 R_2^2 \equiv m^2 R_2^2 - q^2 e_d(\gamma)^2. \tag{7.43}$$

Comparing with (7.40), we see that the BF bound is equivalent to the condition

$$\nu(\gamma)^2 \geq 0. \tag{7.44}$$

Thus:

- $\nu(\gamma)^2 > 0$: the AdS_2 region is stable, and the corresponding IR response is governed by a real scaling exponent;
- $\nu(\gamma)^2 = 0$: the system is marginal and defines a critical surface in parameter space;
- $\nu(\gamma)^2 < 0$: the BF bound is violated and the extremal RN–AdS_4 background is IR-unstable.

Using (7.42), the critical surface $\nu(\gamma_c)^2 = 0$ can be written as

$$\frac{m^2}{6} - q^2\left(\frac{\rho}{6(1+16\gamma_c)}\right)^2 + \frac{1}{4} = 0. \tag{7.45}$$

For fixed m, q, and ρ, this defines a critical Weyl coupling γ_c at which the AdS_2 mode becomes marginal. Near this critical point we can expand

$$\nu(\gamma)^2 \approx a\,(\gamma - \gamma_c), \tag{7.46}$$

for positive constant $a = \frac{8}{9}\frac{q^2\rho^2}{(1+16\gamma_c)^3} > 0$, as long as $1 + 16\gamma_c > 0$, determined by the microscopic parameters. On the unstable side, $\gamma < \gamma_c$, we then have

$$\nu(\gamma) = i\,\lambda(\gamma), \qquad \lambda(\gamma) \equiv \sqrt{-\nu(\gamma)^2} \simeq \sqrt{a(\gamma_c - \gamma)} > 0. \tag{7.47}$$

The IR exponent becomes imaginary, and the AdS_2 mode acquires an oscillatory behavior in $\log\zeta$, as we now discuss.

Physical interpretation of γ_c. A useful physical interpretation emerges when the critical value is chosen to be $\gamma_c = 0$. In that case, the undeformed theory lies exactly at the threshold between two different kinds of low-energy behavior. Small positive and negative values of γ then move the system to opposite sides of the critical point: one side remains in the stable normal phase, while the other is driven toward scalar condensation and the onset of superconductivity. From this point of view, γ plays the role of a tuning parameter around a quantum critical threshold, and the special choice $\gamma_c = 0$ gives that threshold a particularly transparent interpretation. It also makes the sign of γ physically meaningful, allowing one to think of the two sides as favoring different kinds of low-energy response, often described qualitatively as more particle-like or more vortex-like. Near this threshold, the instability generates an IR scale whose exponentially small BKT form will be derived in the next section.

7.4 Efimov tower, and BKT transition

7.4.1 Zero–frequency Schrödinger problem and oscillatory solutions

We now zoom in on the unstable regime $\nu(\gamma)^2 < 0$ identified in Sec. 7.3. Recall that in the near-horizon $AdS_2 \times \mathbb{R}^2$ region the charged scalar obeys the radial equation in Schrödinger form, cf. (7.37)–(7.38). Near the AdS_2 boundary $\zeta \to 0$ the potential is dominated by the inverse-square term and the general solution behaves as (7.39) with exponent $\nu(\gamma)$ defined in (7.40).

On the side where the AdS_2 BF bound is violated we have

$$\nu(\gamma)^2 < 0 \quad \Longrightarrow \quad \nu(\gamma) = i\,\lambda(\gamma), \qquad \lambda(\gamma) \equiv \sqrt{-\nu(\gamma)^2} > 0. \tag{7.48}$$

Writing $\phi(\zeta) = \zeta^{1/2}\chi(\zeta)$, the zero–frequency ($\omega = 0$) equation reduces to the inverse-square Schrödinger problem

$$-\frac{d^2}{d\zeta^2}\chi(\zeta) - \frac{\lambda(\gamma)^2 + \frac{1}{4}}{\zeta^2}\,\chi(\zeta) = 0, \tag{7.49}$$

which is the starting point for the Efimov analysis [16].

7.4.2 Finite AdS_2 throat, Efimov tower and IR scale

In pure AdS_2, ζ runs from 0 to ∞, and whenever $\nu^2 < 0$ there are infinitely many normalizable zero-energy modes, signaling BF violation. In the full RN–AdS_4 geometry, the AdS_2 region is only an intermediate throat: it is valid on a finite interval

$$\zeta \in [\zeta_{\rm UV}, \zeta_{\rm IR}], \tag{7.50}$$

where $\zeta_{\rm UV}$ is defined by matching to the asymptotic AdS_4 region, and $\zeta_{\rm IR}$ is set either by a finite-temperature horizon or by nonlinear effects in the deep IR.

On this finite interval, the zero–frequency mode must satisfy a second boundary condition at $\zeta = \zeta_{\rm IR}$. Taking again Dirichlet $\chi(\zeta_{\rm IR}) = 0$, the oscillatory solution implies

$$\lambda(\gamma)\,\log\frac{\zeta_{\rm IR}}{\zeta_{\rm UV}} = n\pi, \qquad n \in \mathbb{Z}. \tag{7.51}$$

The lowest mode ($n = 1$) has no nodes and corresponds to the onset of instability. For this mode,

$$\log\frac{\zeta_{\rm IR}}{\zeta_{\rm UV}} = \frac{\pi}{\lambda(\gamma)} \quad \Longrightarrow \quad \zeta_{\rm IR} \sim \zeta_{\rm UV}\,\exp\!\Big[\tfrac{\pi}{\lambda(\gamma)}\Big]. \tag{7.52}$$

Since energy scales in AdS_2 are inversely proportional to the radial coordinate, the generated IR scale is

$$\Lambda_{\rm IR} \sim \frac{1}{\zeta_{\rm IR}} \sim \Lambda_{\rm UV}\,\exp\!\Big[-\tfrac{\pi}{\lambda(\gamma)}\Big] = \Lambda_{\rm UV}\,\exp\!\left[-\frac{\pi}{\sqrt{-\nu(\gamma)^2}}\right], \tag{7.53}$$

where $\Lambda_{\rm UV} \sim 1/\zeta_{\rm UV}$ is of order the chemical potential μ. This is exactly the "conformality–lost" scaling derived in [17]: when the BF bound is violated by a small amount $|\nu| \ll 1$, an exponentially small IR scale emerges.

Allowing more oscillations ($n = 2, 3, \ldots$) in (7.51) gives an infinite sequence of IR scales

$$\Lambda_{\rm IR}^{(n)} \sim \Lambda_{\rm UV} \exp\left[-\tfrac{n\pi}{\lambda(\gamma)}\right], \qquad n = 1, 2, \ldots, \tag{7.54}$$

the holographic analogue of an *Efimov tower* of bound states: each higher state is suppressed by an additional factor $\exp[-\pi/\lambda(\gamma)]$.

7.4.3 BKT scaling of the critical temperature

At small but finite temperature the AdS_2 throat is cut off in the IR by the near-extremal horizon at $\zeta = \zeta_h \sim 1/T$. The condition for the onset of the instability is that the horizon lies at or beyond the IR scale of the lowest Efimov mode,

$$\zeta_h \zeta_{\rm IR}^{(1)} \quad \Longleftrightarrow \quad TT_c(\gamma) \sim \frac{1}{\zeta_{\rm IR}^{(1)}}. \tag{7.55}$$

Using (7.52) we obtain the BKT form of the critical temperature:

$$T_c(\gamma) \sim \Lambda_{\rm UV} \exp\left[-\tfrac{\pi}{\lambda(\gamma)}\right] = \Lambda_{\rm UV} \exp\left[-\frac{\pi}{\sqrt{-\nu(\gamma)^2}}\right]. \tag{7.56}$$

Near the critical Weyl coupling γ_c, one has $\nu(\gamma)^2 \simeq a(\gamma - \gamma_c))$ with $a > 0$, so for $\gamma < \gamma_c$ on the unstable side,

$$\lambda(\gamma) \simeq \sqrt{a(\gamma_c - \gamma)}, \tag{7.57}$$

and thus

$$T_c(\gamma) \sim \Lambda_{\rm UV} \exp\left[-\frac{\pi}{\sqrt{a(\gamma_c - \gamma)}}\right], \tag{7.58}$$

in direct analogy with the holographic BKT transitions studied in [16]. Here the role of $(m_c^2 - m^2)$ is played by $-\nu(\gamma)^2$, which encodes both the bare mass and the Weyl-renormalized electric coupling $qe_d(\gamma)$.

7.5 IR Green's function in AdS$_2$

The AdS$_2$ analysis of Sec. 7.3 also determines the low-frequency behavior of the IR retarded Green's function. Using the near-boundary expansion (7.39) with exponent $\nu(\gamma)$ in (7.40), we write

$$\phi_\omega(\zeta) = A(\omega)\,\zeta^{\frac{1}{2}-\nu(\gamma)}\big(1+\mathcal{O}(\zeta)\big) + B(\omega)\,\zeta^{\frac{1}{2}+\nu(\gamma)}\big(1+\mathcal{O}(\zeta)\big), \tag{7.59}$$

where $A(\omega)$ and $B(\omega)$ are fixed by imposing ingoing boundary conditions at the AdS$_2$ horizon. Solving the full AdS$_2$ problem [15] one finds

$$A(\omega) \sim \omega^{\frac{1}{2}-\nu(\gamma)}, \qquad B(\omega) \sim \omega^{\frac{1}{2}+\nu(\gamma)}. \tag{7.60}$$

In the emergent AdS$_2$/CFT$_1$ description, the IR response is encoded in the ratio of the normalizable to non-normalizable coefficients. Therefore,

$$G^R_{\mathrm{IR}}(\omega;\gamma) \equiv \frac{B(\omega)}{A(\omega)} \propto \omega^{2\nu(\gamma)}, \qquad \omega \to 0. \tag{7.61}$$

When the AdS$_2$ BF bound is satisfied, $\nu(\gamma)$ is real and positive and G^R_{IR} shows a power-law IR response. When the bound is violated, $\nu(\gamma) = i\lambda(\gamma)$ becomes imaginary and

$$G^R_{\mathrm{IR}}(\omega;\gamma) \propto \omega^{2i\lambda(\gamma)} = e^{2i\lambda(\gamma)\log\omega}, \tag{7.62}$$

which is oscillatory in $\log\omega$ and reflects the Efimov tower of IR scales derived in Sec. 7.4.

In the next chapter we will analyze the full holographic setup, compute the retarded Green's functions of the boundary current, and study how the Weyl coupling γ modifies the frequency dependence of the optical conductivity $\sigma(\omega)$.

Chapter 8

Conductivity and Transport

In this chapter we compute the optical conductivity $\sigma(\omega)$ of the boundary theory in the presence of the Weyl coupling γ. We work with linearized fluctuations of the bulk gauge field and extract the retarded Green's function of the boundary current via the standard holographic dictionary. The effect of γ is entirely encoded in how it modifies the bulk equation for the transverse gauge fluctuation A_x, while the UV definition of $\sigma(\omega)$ remains unchanged.

Although the fluctuation equation can be written for a general planar black brane (including RN–AdS$_4$), for our purposes it is sufficient and numerically simpler to work in the probe limit on a fixed Schwarzschild–AdS$_4$ geometry. In this setting, the Weyl coupling γ already produces a nontrivial, frequency-dependent conductivity, both in the normal phase and, when a background scalar profile is present, in the superconducting phase. We will comment on how the results generalize to RN–AdS$_4$ and connect to the IR analysis of Chapter 7.

Throughout we keep the dimensionless conventions of Section 6.3,

$$L = 1, \qquad r_h = 1. \tag{8.1}$$

8.1 Fluctuation Analysis

8.1.1 Background and perturbation ansatz

We consider the planar Schwarzschild–AdS$_4$ black brane,

$$ds^2 = -f(r)\,dt^2 + \frac{dr^2}{f(r)} + r^2(dx^2 + dy^2), \tag{8.2}$$

with

$$f(r) = r^2\left(1 - \frac{1}{r^3}\right) = r^2 - \frac{1}{r}, \tag{8.3}$$

so that the horizon is at $r = 1$ and the temperature is

$$T = \frac{f'(1)}{4\pi} = \frac{3}{4\pi}. \tag{8.4}$$

For the conductivity computation we study the linear response to a small electric field along the x-direction. In the normal phase this reduces to a neutral-plasma calculation with $\psi = 0$, while in the superconducting phase the same fluctuation is studied on top of nontrivial background matter fields in the probe-limit Schwarzschild–AdS$_4$ geometry.

We now perturb the bulk gauge field by a transverse fluctuation

$$\delta A_x(t, r) = A_x(r)\, e^{-i\omega t}, \tag{8.5}$$

with all other components set to zero and no spatial momentum ($k_x = k_y = 0$). We keep the scalar profile $\psi(r)$ general in the intermediate steps, so that the same fluctuation equation applies both in the normal phase ($\psi = 0$) and in the superconducting phase ($\psi \neq 0$). In practice, to isolate the role of γ in the conductivity we will often set $\psi = 0$.

8.1.2 Weyl-corrected Maxwell equations for A_x

The Maxwell equation with the Weyl correction (from (6.6)) reads

$$\nabla_\mu \big(F^{\mu\nu} - 4\gamma\, C^{\mu\nu\rho\sigma} F_{\rho\sigma} \big) = 2\psi^2 A^\nu, \tag{8.6}$$

where the right-hand side corresponds to the effective Proca mass term induced by the scalar condensate.[1]

For the metric (8.2), the nonzero Weyl components relevant for the fluctuation are

$$C_{rxrx} = \frac{r^2 f'' - 2rf' + 2f}{12 f}, \qquad C_{txtx} = -\frac{f}{12}\big(r^2 f'' - 2rf' + 2f\big). \tag{8.7}$$

It is convenient to introduce the scalar function

$$K(r) \equiv C^{rtrt} = \frac{2f - 2rf' + r^2 f''}{6r^2}, \tag{8.8}$$

[1]The precise coefficient depends on the normalization of the scalar kinetic term and the charge; here we adopt the convention consistent with the equations in Chapter 6. In the normal phase $\psi = 0$ and the right-hand side vanishes.

which also appeared in the IR analysis of Chapter 7. In terms of $K(r)$, the components (8.7) can be reexpressed, and the Weyl contributions to the fluctuation equation become compact.

Inserting the ansatz (8.5) into (8.6), and using the expressions for the field strengths F^{rx}, F^{tx} and the Weyl contractions $C^{\mu\nu\rho\sigma}F_{\rho\sigma}$, one finds after some algebra that the $\nu = x$ component reduces to the radial ordinary differential equation

$$\partial_r\big(f(r)\,[1-4\gamma K(r)]\,A_x'(r)\big) + [1-4\gamma K(r)]\,\frac{\omega^2}{f(r)}\,A_x(r) = 2\psi^2(r)\,A_x(r). \tag{8.9}$$

This equation is valid for any planar blackening factor $f(r)$ of the form (8.2); in particular, it applies equally well to the RN–AdS$_4$ background used in Chapter 7 upon replacing $f(r)$ and $K(r)$ by their RN expressions. Here we specialize to the Schwarzschild–AdS$_4$ case (8.3) for simplicity.

In the normal phase $\psi = 0$, the equation simplifies to

$$\partial_r\big(f(r)\,[1-4\gamma K(r)]\,A_x'(r)\big) + [1-4\gamma K(r)]\,\frac{\omega^2}{f(r)}\,A_x(r) = 0. \tag{8.10}$$

It is useful to recognize (8.10) as a Sturm–Liouville-type equation,

$$\partial_r\big(\Pi(r)\,A_x'(r)\big) + \omega^2\,W(r)\,A_x(r) = 0, \tag{8.11}$$

with

$$\Pi(r) = f(r)\,[1-4\gamma K(r)], \qquad W(r) = \frac{1-4\gamma K(r)}{f(r)}. \tag{8.12}$$

The factor $1-4\gamma K(r)$ plays the role of a radial, Weyl-induced dielectric function.

In the superconducting phase ($\psi \neq 0$), the right-hand side of (8.9) provides an additional effective mass term $\propto \psi^2(r)A_x(r)$. The structure (8.11) is preserved, with a potential term coming from the condensate.

8.2 Green's function and Kubo formula

The extraction of the retarded Green's function and the conductivity closely parallels the discussion in Section 4.3. Here we simply summarize the key steps.

8.2.1 Boundary conditions

Horizon. Regularity at the future horizon requires an ingoing wave in Eddington–Finkelstein coordinates. Near $r = 1$ this implies

$$A_x(r) \sim (r-1)^{-i\omega/(4\pi T)}, \qquad T = \frac{3}{4\pi}. \tag{8.13}$$

This condition fixes the solution of (8.9) up to an overall normalization.

Boundary. As $r \to \infty$, the Weyl tensor decays and $K(r) \to 0$. The fluctuation equation therefore reduces to the standard Maxwell equation in AdS_4, and the solution has the familiar asymptotic expansion

$$A_x(r) = A_x^{(0)}(\omega) + \frac{A_x^{(1)}(\omega)}{r} + \mathcal{O}\left(\frac{1}{r^2}\right). \tag{8.14}$$

In the AdS/CFT dictionary, $A_x^{(0)}$ is the source for the boundary current J_x, while $A_x^{(1)}$ is proportional to the expectation value $\langle J_x \rangle$.

The important point is that the Weyl term does *not* modify this UV structure: all γ-dependence vanishes too fast near the boundary to affect the leading and subleading coefficients in (8.14). All dependence on γ enters only through how (8.9) propagates the fluctuation from the horizon to the boundary.

8.2.2 Retarded Green's function and conductivity

To extract the retarded Green's function we evaluate the quadratic action for A_x on-shell. Starting from the gauge-field part of the action

$$S_A = -\frac{1}{4}\int d^4x\, \sqrt{-g}\left(F_{\mu\nu}F^{\mu\nu} - 4\gamma\, C^{\mu\nu\rho\sigma}F_{\mu\nu}F_{\rho\sigma}\right), \tag{8.15}$$

and integrating by parts, one finds that on-shell the bulk term vanishes and only boundary terms remain:

$$S_A^{\text{on-shell}} = -\frac{1}{2}\int_{\partial\mathcal{M}} d^3x\sqrt{-h}\left(F^{\mu\nu} - 4\gamma\, C^{\mu\nu\rho\sigma}F_{\rho\sigma}\right)n_\mu A_\nu, \tag{8.16}$$

where h is the induced metric on the boundary and n_μ the outward unit normal.

For our fluctuation $\delta A_x(t,r)$ in the background (8.2), only the $(\mu,\nu) = (r,x)$

component contributes at the UV boundary:

$$S_A^{\text{on-shell}} = -\frac{1}{2}\int d^3x\,\sqrt{-h}\left(F^{rx} - 4\gamma\, C^{rx\rho\sigma}F_{\rho\sigma}\right) n_r A_x. \tag{8.17}$$

Using the explicit expressions for F^{rx}, $C^{rx\rho\sigma}$ and the metric, one can show that the Weyl term falls off sufficiently fast that it does not contribute at the UV boundary:

$$C^{rx\rho\sigma}F_{\rho\sigma}\big|_{r\to\infty} \;\to\; 0. \tag{8.18}$$

Thus the on-shell action reduces near the boundary to the familiar form

$$S_A^{\text{on-shell}} = -\frac{1}{2}\int d^3x\, A_x(r,\omega)\, f(r)\,\partial_r A_x(r,-\omega)\Big|_{r\to\infty}, \tag{8.19}$$

up to an overall normalization that we fix by matching to the standard AdS/CFT dictionary.

Varying (8.19) with respect to the boundary value $A_x^{(0)}$ gives the retarded Green's function

$$G^R(\omega) = -\lim_{r\to\infty} f(r)\,\frac{\partial_r A_x(r,\omega)}{A_x(r,\omega)}. \tag{8.20}$$

Using the expansion (8.14) and the fact that $f(r) \sim r^2$ as $r \to \infty$, we obtain

$$G^R(\omega) = -\frac{A_x^{(1)}(\omega)}{A_x^{(0)}(\omega)}. \tag{8.21}$$

This relation is structurally identical to the $\gamma = 0$ case; the Weyl coupling modifies only the bulk equation that determines the ratio $A_x^{(1)}/A_x^{(0)}$.

8.2.3 Kubo formula and conductivity

The optical conductivity $\sigma(\omega)$ is given by the Kubo formula

$$\sigma(\omega) = \frac{1}{i\omega}G^R(\omega). \tag{8.22}$$

Combining (8.22) with (8.21), we arrive at

$$\sigma(\omega) = -\frac{1}{i\omega}\frac{A_x^{(1)}(\omega)}{A_x^{(0)}(\omega)}. \tag{8.23}$$

Up to overall sign conventions relating the electric field $E_x = -\partial_t A_x^{(0)} = i\omega A_x^{(0)}$ and the current $J_x \sim A_x^{(1)}$, the conductivity is thus determined by the ratio of the subleading to leading coefficients in the near-boundary expansion of the bulk solution.

In practice, the computation proceeds as follows:

1. Impose the ingoing boundary condition (8.13) at the horizon and integrate the ODE (8.10) (or the full equation with $\psi \neq 0$) outward to large r.
2. Read off $A_x^{(0)}(\omega)$ and $A_x^{(1)}(\omega)$ from the asymptotic expansion (8.14).
3. Form the ratio $A_x^{(1)}/A_x^{(0)}$ and insert it into (8.23).

Repeating this procedure for different frequencies ω yields the full frequency-dependent conductivity $\sigma(\omega)$.

8.3 Optical conductivity and the role of γ

8.3.1 Self–dual case $\gamma = 0$

For $\gamma = 0$, the bulk theory reduces to ordinary Maxwell theory on Schwarzschild–AdS$_4$. As reviewed in Chapter 5, this theory is electromagnetically self–dual, and in the homogeneous, translation–invariant set-up considered here this implies a frequency–independent optical conductivity,

$$\Re\sigma(\omega) = \sigma_0, \qquad \Im\sigma(\omega) = 0, \tag{8.24}$$

up to contact terms. Numerically, solving (8.10) with $\gamma = 0$ reproduces a flat real part of $\sigma(\omega/T)$, as illustrated in Figure 4.1.

8.3.2 Turning on γ: particle vs. vortex response

When $\gamma \neq 0$, the Weyl coupling breaks EM self–duality in the bulk, and the factor $1 - 4\gamma K(r)$ in (8.12) distorts the radial propagation of the transverse mode. The resulting conductivity develops a nontrivial frequency dependence even in the absence of a lattice or impurities.

Figure 8.1 shows the real part of the conductivity for representative positive and negative values of γ, separately for the two quantizations. The qualitative trend is the same in both cases:

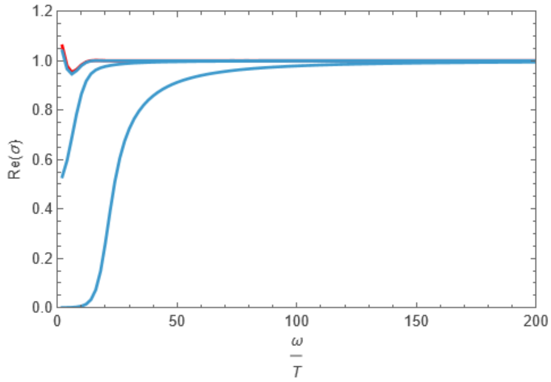

(a) $\gamma > 0$, $\Delta = 1$

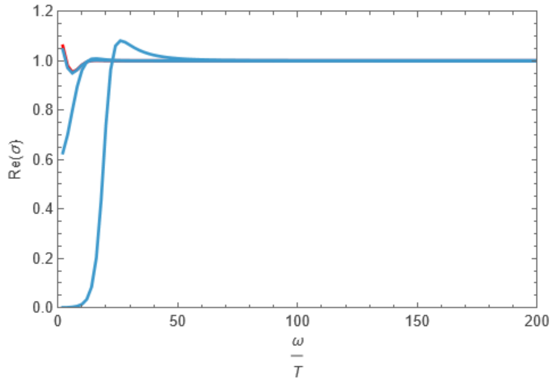

(b) $\gamma > 0$, $\Delta = 2$

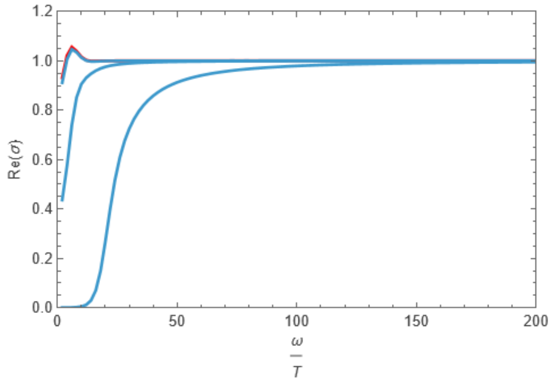

(c) $\gamma < 0$, $\Delta = 1$

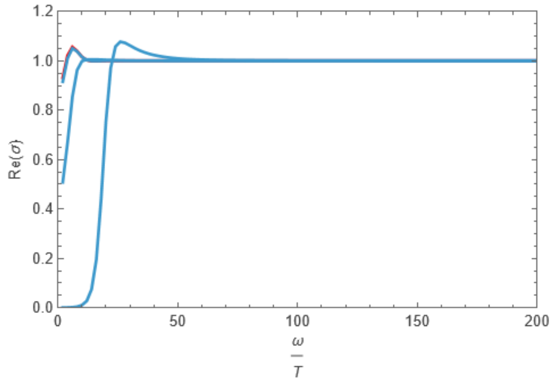

(d) $\gamma < 0$, $\Delta = 2$

Figura 8.1: Optical conductivity on Schwarzschild–AdS$_4$ with Weyl corrections. Real part $\Re\sigma(\omega/T)$ for representative positive and negative γ, shown separately for the two quantizations ($\Delta = 1$ and $\Delta = 2$). Each panel contains several temperature curves: the red curve (only partially visible due to overlap with the others) corresponds to the profile at $T = T_c$, while the remaining curves show successively lower temperatures $T < T_c$. Positive γ enhances the low-frequency response, whereas negative γ suppresses it.

- For $\gamma > 0$, $\Re\sigma(\omega/T)$ exhibits a mild enhancement at low frequency, reminiscent of a broadened Drude peak and suggestive of a particle–like transport channel.

- For $\gamma < 0$, the low–frequency response is suppressed and can develop a dip or minimum, which is naturally interpreted as a vortex–like channel dominating the IR dynamics.

The high–frequency limit $\omega/T \to \infty$ is insensitive to γ, as expected from the fact that the Weyl tensor vanishes near the AdS boundary and the UV conductivity is controlled by the self–dual Maxwell theory.

In RN–AdS_4, the same machinery applies with a different blackening factor $f(r)$ and curvature function $K(r)$. In that case, the low–frequency, low–temperature behavior of $\sigma(\omega)$ is controlled by the IR scaling dimension $\Delta_{\mathrm{IR}}(\gamma)$ of the charged mode in the $\mathrm{AdS}_2 \times \mathbb{R}^2$ throat (Chapter 7), and the Weyl coupling γ not only reshapes $\sigma(\omega)$ but also tunes the BKT scale $T_c(\gamma)$. We will come back to this connection in the concluding chapter.

Chapter 9

Discussion and Outlook

In this final chapter we summarize the main results of the thesis, interpret them from a condensed–matter perspective (with an eye on strange metals and quantum criticality), and outline directions for future work. We emphasize which features are universal and which are artefacts or limitations of the simplified holographic model.

9.1 Summary of Main Results

The starting point of this work is an Einstein–Maxwell–scalar model in AdS_4, describing a holographic superconductor, deformed by a higher–derivative Weyl coupling in the gauge sector,

$$\Delta S_{\text{Weyl}} = \gamma L^2 \int d^4x \sqrt{-g}\, C_{\mu\nu\rho\sigma} F^{\mu\nu} F^{\rho\sigma}, \tag{9.1}$$

treated perturbatively in the small–γ regime. To the order considered here, the background geometry is kept fixed while the Maxwell equations and, consequently, transport are modified.

The main results can be grouped into two closely related themes.

(i) IR data, BF bound, and BKT–type criticality

In the normal phase, the near–horizon region of the extremal Reissner–Nordström–AdS_4 black brane is $AdS_2 \times \mathbb{R}^2$. In this AdS_2 throat, the charged scalar feels an effective mass and electric coupling that depend on γ. This leads to a γ–dependent IR scaling dimension $\delta(\gamma) = \frac{1}{2} + \nu(\gamma)$ in the emergent CFT_1, with $\nu(\gamma)$ controlled by the effective AdS_2 mass and charge.

As γ is varied, the effective mass can violate the AdS_2 BF bound while the scalar mass still satisfies the AdS_4 BF bound in the UV. The locus $\nu(\gamma)^2 = 0$ defines a quantum critical surface in parameter space. In the interpretation adopted in this thesis, the special choice $\gamma_c = 0$ means that the undeformed theory sits exactly at this threshold, so that the sign of γ directly labels the two sides of the quantum critical point. For $\nu(\gamma)^2 < 0$, the normal phase becomes unstable at $T = 0$, signaling the onset of a superconducting phase.

Close to this critical surface, the critical temperature behaves as

$$T_c(\gamma) \sim \Lambda \exp\left(-\frac{\pi}{\sqrt{-\nu(\gamma)^2}}\right), \tag{9.2}$$

with Λ a suitable UV scale. This essential singularity is characteristic of a BKT–type transition, in contrast with the mean–field power laws of the minimal holographic superconductor. One of the key messages of the thesis is that the Weyl coupling γ provides a simple holographic knob to engineer such non–mean–field, BKT–like quantum criticality in a controlled and geometrically transparent way.

(ii) Conductivity and particle–vortex asymmetry

The same Weyl coupling also leaves a clear imprint on transport. By turning on transverse gauge fluctuations $A_x(r)e^{-i\omega t}$ and solving their radial equation with ingoing boundary conditions at the horizon, we computed the optical conductivity $\sigma(\omega)$ via the usual holographic Kubo formula.

On a fixed Schwarzschild–AdS$_4$ background, this analysis shows that:

- For $\gamma = 0$, electromagnetic self–duality of the bulk Maxwell sector enforces a frequency–independent optical conductivity $\Re\sigma(\omega) = \text{const}$, in agreement with previous work.

- For $\gamma \neq 0$, the Weyl term introduces a curvature–dependent factor in the fluctuation equation that breaks EM self–duality. The result is a genuinely frequency–dependent $\sigma(\omega)$ even in a homogeneous, translation–invariant background.

- The sign of γ determines whether the low–frequency response is more particle–like (enhanced low–ω spectral weight for $\gamma > 0$) or more vortex–like (suppressed low–ω response for $\gamma < 0$), while the UV/high–frequency behavior is essentially insensitive to γ because the Weyl tensor dies off in the asymptotic AdS region.

On a charged RN–AdS$_4$ background, the linear-response analysis proceeds analogously at the level of the bulk fluctuation problem: the Weyl term enters through the same curvature-dependent factor $1 - 4\gamma K(r)$, but with $f(r)$ and $K(r)$ replaced by their RN expressions, and in general finite density can introduce mixing with metric perturbations. A full quantitative determination of how these ingredients reshape the optical spectrum in the charged/superconducting case is left for future numerical work.

9.2 Condensed–Matter Interpretation

The analysis above can be rephrased in purely condensed–matter language.

γ as an effective control parameter

On the gravity side, γ multiplies a higher–derivative interaction between the gauge sector and curvature. In the near–horizon AdS_2 region this translates into a renormalization of the IR electric coupling $e_d(\gamma)$, which determines the scaling dimension of the order parameter and whether the BF bound is violated.

From the boundary perspective, γ thus behaves as an abstract *control knob* that tunes the low–energy universality class of the system: it moves the theory across a quantum critical surface, changes the scaling of the order parameter, and controls whether the superconducting transition is mean–field–like or BKT–like. This is qualitatively similar to how carrier density, disorder, pressure, or dielectric environment tune real materials across quantum critical points.

The key point, compared to earlier holographic BKT constructions where one typically tunes an abstract bulk scalar mass or charge, is that here the control parameter γ is a *physical* higher–derivative coupling in the gauge sector. It simultaneously breaks electromagnetic self–duality and biases the response toward more particle–like or more vortex–like transport behavior. Because similar CFF-type structures appear in ABJM–inspired and Landau–Ginzburg–like effective descriptions, the Weyl–corrected holographic superconductor is a more realistic candidate to model intertwined quantum and thermal transitions near a critical point, rather than an entirely ad hoc engineering of BKT behavior.

Connection to strange metals and quantum criticality

Strange metals and unconventional superconductors often appear near putative $T = 0$ quantum critical points, with non–Fermi–liquid transport and broad, incoherent optical spectra. The holographic model studied here reproduces several ingredients that are useful for modeling this situation:

- a strongly coupled normal state without quasiparticles (realized holographically by a charged black brane);
- an emergent IR fixed point (AdS_2) that controls low–energy scaling;
- a tunable parameter γ that drives a quantum critical surface and BKT–type scaling of T_c;
- a nontrivial optical conductivity $\sigma(\omega)$ with significant redistribution of spectral weight and controllable particle–vortex asymmetry.

At the same time, the model is highly idealized: it lacks explicit fermions and a microscopic Fermi surface, has exact translational invariance (and hence infinite DC conductivity) unless momentum relaxation is added by hand, and contains no explicit vortices or lattice degrees of freedom. The intended interpretation is therefore that of a universal, strongly coupled toy model capturing qualitative aspects of quantum critical superconductivity and strange–metal transport, rather than a faithful description of any particular material.

9.3 Lessons for Holography and Strongly Coupled Matter

Beyond the specific computations, the thesis illustrates a few general points.

First, holography provides a unified geometric language for a variety of phase transitions: by adjusting the IR geometry and effective couplings (here via the Weyl term), one can interpolate between mean–field transitions and BKT–type criticality within the same basic framework of black branes, IR throats and BF bounds.

Second, higher–derivative terms that are naively "small corrections" in the UV can qualitatively reorganize IR physics when they couple to fields that dominate near the horizon. In our case, the Weyl coupling leaves the UV AdS_4 region essentially unchanged but strongly affects the AdS_2 throat and the transport sector.

Finally, the analysis clarifies the split between universal and microscopic information in bottom–up holographic models: IR scaling exponents, the existence of a QCP, and the broad structure of $\sigma(\omega)$ are robust and largely independent of the UV completion, while material–specific features (band structure, detailed gap symmetry, vortex lattices) lie outside the scope of the present setup.

9.4 Outlook

Several natural extensions of this work suggest themselves.

Momentum relaxation and disorder. Introducing momentum relaxation (for instance via Q–lattices, spatially dependent scalar fields, or massive gravity constructions) would allow a finite DC conductivity in the normal phase and a more realistic comparison to strange–metal transport. It would be interesting to study how the interplay between γ and momentum relaxation affects low–frequency transport and possible scaling relations.

Fermionic probes and Fermiology. Coupling probe fermions to the Weyl–corrected background would make it possible to study spectral functions and potential holographic Fermi surfaces near the BKT–type quantum critical point, and to ask how γ modifies non–Fermi–liquid behavior and quasiparticle residues.

Beyond the probe limit. Relaxing the probe approximation and including full backreaction of the Weyl term and condensate on the geometry would clarify how robust the AdS_2 IR fixed point and the associated BKT scaling remain, and whether additional constraints on γ arise from regularity, causality or positivity when the geometry is fully dynamical.

Magnetic fields and vortices. To connect more directly with BKT physics in thin films, it would be natural to introduce an external magnetic field, construct vortex or vortex–lattice solutions in the presence of the Weyl term, and investigate whether the BKT–like scaling obtained from the AdS_2 analysis can be related to vortex–antivortex physics in an appropriate dual description.

Taken together, the results of this thesis show that a single higher–derivative parameter γ in a simple holographic model already suffices to tune IR critical exponents, trigger BKT–type quantum criticality, and reshape strong–coupling transport. This fits into a broader theme of AdS/CFT: modest deformations of the bulk action can encode nontrivial reorganizations of the low–energy physics on the boundary, making holography a useful laboratory for exploring universality classes that are difficult to access by conventional methods.

References

[1] Juan M. Maldacena. The large n limit of superconformal field theories and supergravity. *Advances in Theoretical and Mathematical Physics*, 2:231–252, 1998. Int. J. Theor. Phys. **38**, 1113–1133 (1999).

[2] Horatiu Nastase. *Introduction to the AdS/CFT Correspondence*. Cambridge University Press, Cambridge, 2015.

[3] Horatiu Nastase. *String Theory Methods for Condensed Matter Physics*. Cambridge University Press, Cambridge, 2017.

[4] Steven S. Gubser. Breaking an abelian gauge symmetry near a black hole horizon. *Physical Review D*, 78:065034, 2008.

[5] Sean A. Hartnoll, Christopher P. Herzog, and Gary T. Horowitz. Holographic superconductors. *Journal of High Energy Physics*, 12:015, 2008.

[6] Sean A. Hartnoll. Lectures on holographic methods for condensed matter physics. *Classical and Quantum Gravity*, 26:224002, 2009.

[7] Robert C. Myers, Subir Sachdev, and Ajay Singh. Holographic quantum critical transport without self-duality. *Physical Review D*, 83:066017, 2011.

[8] Subir Sachdev. What can gauge-gravity duality teach us about condensed matter physics? *Annual Review of Condensed Matter Physics*, 3:9–33, 2012.

[9] Sean A. Hartnoll, Andrew Lucas, and Subir Sachdev. Holographic quantum matter. 2016.

[10] Juan Maldacena, Stephen H. Shenker, and Douglas Stanford. A bound on chaos. *Journal of High Energy Physics*, 2016(8):106, 2016.

[11] Petter Minnhagen. The two-dimensional coulomb gas, vortex unbinding, and superfluid-superconducting films. *Reviews of Modern Physics*, 59(4):1001–1066, 1987.

[12] Sean A. Hartnoll, Christopher P. Herzog, and Gary T. Horowitz. Building a holographic superconductor. *Physical Review Letters*, 101:031601, 2008.

[13] Peter Breitenlohner and Daniel Z. Freedman. Stability in gauged extended supergravity. *Annals of Physics*, 144:249–281, 1982.

[14] Christopher P. Herzog, Pavel Kovtun, Subir Sachdev, and Dam T. Son. Quantum critical transport, duality, and m-theory. *Physical Review B*, 75:085103, 2007.

[15] Thomas Faulkner, Hong Liu, John McGreevy, and David Vegh. Emergent quantum criticality, fermi surfaces, and ads_2. *Physical Review D*, 83(12):125002, 2011.

[16] Nabil Iqbal, Hong Liu, Márk Mezei, and Qimiao Si. Quantum phase transitions in holographic models of magnetism and superconductors. *Physical Review D*, 82:045002, 2010.

[17] David B. Kaplan, Jong-Wan Lee, Dam T. Son, and Mikhail A. Stephanov. Conformality lost. *Physical Review D*, 80:125005, 2009.